Archives of Biochemistry and Biophysics 622 (2017) 9–25

Contents lists available at ScienceDirect

Archives of Biochemistry and Biophysics

journal homepage: www.elsevier.com/locate/yabbi

Tyrosine oxidation and nitration in transmembrane peptides is connected to lipid peroxidation

Silvina Bartesaghi [a, b, c, *], Daniel Herrera [a, c, 1], Débora M. Martinez [a, c, 1], Ariel Petruk [e], Verónica Demicheli [a, c], Madia Trujillo [a, c], Marcelo A. Martí [d], Darío A. Estrín [e], Rafael Radi [a, c, **]

[a] Departamento de Bioquímica, Facultad de Medicina, Universidad de la República, Avda. Gral. Flores 2125, Montevideo 11800, Uruguay
[b] Departamento de Educación Médica, Facultad de Medicina, Universidad de la República, Avda. Gral. Flores 2125, Montevideo 11800, Uruguay
[c] Center for Free Radical and Biomedical Research, Facultad de Medicina, Universidad de la República, Avda. Gral. Flores 2125, Montevideo 11800, Uruguay
[d] Departamento de Química Biológica and IQUIBICEN-CONICET, Facultad de Ciencias Exactas y Naturales, Universidad de Buenos Aires, Cuidad Universitaria, Pab 2, C1428EHA, Buenos Aires, Argentina
[e] Departamento de Química Inorgánica, Analítica y Química-Física and INQUIMAE-CONICET, Facultad de Ciencias Exactas y Naturales, Universidad de Buenos Aires, Cuidad Universitaria, Pab 2, C1428EHA, Buenos Aires, Argentina

ARTICLE INFO

Article history:
Received 29 November 2016
Received in revised form
7 April 2017
Accepted 11 April 2017
Available online 13 April 2017

Keywords:
Tyrosine nitration
Peroxynitrite
Liposomes
Membranes
Lipid peroxidation
Free radicals

ABSTRACT

Tyrosine nitration is an oxidative post-translational modification that can occur in proteins associated to hydrophobic bio-structures such as membranes and lipoproteins. In this work, we have studied tyrosine nitration in membranes using a model system consisting of phosphatidylcholine liposomes with pre-incorporated tyrosine-containing 23 amino acid transmembrane peptides. Tyrosine residues were located at positions 4, 8 or 12 of the amino terminal, resulting in different depths in the bilayer. Tyrosine nitration was accomplished by exposure to peroxynitrite and a peroxyl radical donor or hemin in the presence of nitrite. In egg yolk phosphatidylcholine liposomes, nitration was highest for the peptide with tyrosine at position 8 and dramatically increased as a function of oxygen levels. Molecular dynamics studies support that the proximity of the tyrosine phenolic ring to the linoleic acid peroxyl radicals contributes to the efficiency of tyrosine oxidation. In turn, α-tocopherol inhibited both lipid peroxidation and tyrosine nitration. The mechanism of tyrosine nitration involves a "connecting reaction" by which lipid peroxyl radicals oxidize tyrosine to tyrosyl radical and was fully recapitulated by computer-assisted kinetic simulations. Altogether, this work underscores unique characteristics of the tyrosine oxidation and nitration process in lipid-rich milieu that is fueled *via* the lipid peroxidation process.

1. Introduction

Protein tyrosine nitration is a post-translational modification mediated by nitric oxide (•NO)-derived oxidants such as peroxynitrite ($ONOO^-$/ONOOH) and nitrogen dioxide ($•NO_2$) [1–3]. Protein tyrosine nitration is a well-recognized oxidative modification, leading to a number of functional consequences that may include either a gain- or a loss-of-protein function. The main mechanism of protein tyrosine nitration *in vivo* is based on free radical reactions that involve the intermediate formation of the tyrosyl radical (•Tyr) followed by the addition of $•NO_2$, leading to 3-nitrotyrosine (3-NT) formation [4,5]. Oxidation of tyrosine to tyrosyl radical can be achieved by a number of oxidants such as peroxynitrite-derived radicals (*i.e.* $•NO_2$, hydroxyl (•OH) and carbonate radicals ($CO_3^{•-}$) [6–8], lipid-derived alkoxyl (LO•) and peroxyl (LOO•) radicals [9,10] myeloperoxidase- or transition metal complexes-dependent reactions [5,11,12]. Protein 3-nitrotyrosine represents a footprint of nitro-oxidative modifications *in vivo* [2,13,14], being revealed as a strong biomarker and predictor of disease onset and progression [15–17]. Additionally, a number of tyrosine-nitrated proteins undergo significant changes in protein structure and function as a consequence of tyrosine nitration [4,18,19], with this process being part of pathophysiological pathways [20].

Most of the mechanistic studies of tyrosine nitration for free

* Corresponding author.
** Corresponding author.
E-mail addresses: sbartesa@fmed.edu.uy (S. Bartesaghi), rradi@fmed.edu.uy (R. Radi).
[1] Both authors listed in alphabetic order contributed equally to the paper.

http://dx.doi.org/10.1016/j.abb.2017.04.006
0003-9861/

tyrosine or tyrosine analogs (*e.g.* *p*-hydroxyphenyl acetic acid), tyrosine-containing peptides or proteins have been performed in aqueous solution [13,21–24]. However, in many cases, tyrosine nitration occurs in proteins associated to non-polar or hydrophobic bio-structures as indicated by early work in atherosclerotic plaque [25] and more recently in biomembranes [26–28] and lipoproteins [15–17]. Indeed, the first *in vivo* report detecting nitrated proteins in a human disease condition was performed in an atherosclerotic human coronary artery by immunohistochemistry, where a significant portion of protein-3-nitrotyrosine was associated to a portion of the atheroma plaque rich in lipids. Later on, it was demonstrated that both, Apo A [29] and to a lesser extent Apo B [30] are nitrated *in vitro* and *in vivo* and that apolipoprotein nitration increases in cardiovascular patients, correlating well with the severity of the disease and effectiveness of the treatment [17,31–34]. Several examples of tyrosine nitration in specific membrane proteins have been revealed. Within these proteins, nitration may occur in hydrophobic domains but also in solvent-exposed tyrosine residues. Nitration was demonstrated in several proteins at the plasmatic (*e.g.* erythrocyte membrane band 3 [35,36], mitochondrial (*e.g.* complex I of the inner membrane [37,38]), sarcoplasmic reticulum (*e.g.* Ca^{2+}-ATPase, SERCA [39–42]) and microsomal membranes (*e.g.* glutathione-*S*-transferase [43]). Although with the structural data available is sometimes difficult to assign the position of a tyrosine within a protein associated to hydrophobic environment because not in all cases the native three-dimensional structure is available, in some cases this information exists or can be inferred. The versatile physicochemical properties of tyrosine in virtue of its amphipatic phenolic side chain result in an intermediate hydropathy value in comparison with the rest of the amino acids [44]; thus, tyrosine is capable to interact with both polar or non polar environments [2,4,45]. For example, in the case of SERCA, Tyr 294 and 295, located on a transmembrane domain are nitrated, both *in vitro* and *in vivo*; indeed, the specific nitration of SERCA at Tyr 294 and 295, has been reported in arteries and skeletal muscle during vascular degeneration and aging in both animals and human patients [39,40]. In the case of erythrocyte membrane band 3, tyrosine nitration occurs in the cytosolic, solvent-exposed region but not in the transmembrane domain [35]. For microsomal glutathione *S*-transferase, Tyr 92 close to the active site and on a transmembrane domain becomes nitrated; nitration may be catalyzed by the heme center and would be responsible for the reported gain-of-function [43]. Finally, in apoA-1 the nitration of Tyr 192 [29,46] and Tyr 166 [17] can be modulated by their association to lipids and result in selective functional impairment. Numerous of the physicochemical factors controlling protein tyrosine nitration in hydrophobic bio-structures differ from those in aqueous solution. For instance, the large amount of unsaturated fatty acids present in membranes compete with the protein tyrosine residues for the primary free radical species; other unique characteristics are the exclusion of antioxidants normally present in aqueous phases (*e.g.* glutathione, a strong inhibitor of nitration reactions [47] and the preferential partitioning of nitrating species such as $\bullet NO_2$ and •NO in lipid phases. Our previous studies using a hydrophobic tyrosine analog (*N*-*t*-BOC L-tyrosine *tert* butyl ester, BTBE) incorporated into liposomes [9,48] or red cell membranes [28] and exposed to oxidizing and nitrating systems, revealed that lipid peroxidation could fuel tyrosine oxidation reactions due to the reaction of LOO• radicals with tyrosine to yield •Tyr, that could subsequently be nitrated *via* the termination reaction with $\bullet NO_2$. Thus, we proposed a "connection" between the lipid peroxidation and tyrosine oxidation process in membranes. However, these initial studies performed using BTBE have as limitation the fact that this single amino acid analog is preferentially located in the more hydrophilic area of the membrane and capable to diffuse reasonably through the bilayer [49], processes less likely to occur in tyrosine residues that are part of transmembrane-protein domains.

Thus, in the present work, we have used as hydrophobic tyrosine probes, a series of 23-amino acid polypeptides incorporated to liposomes as transmembrane peptides containing a single tyrosine residue located at different positions from the amino-terminal (Y4, Y8, Y12 [50]) to confirm and further characterize the connection between the lipid an protein oxidation processes; the organization of the transmembrane peptides within the liposomal membranes recapitulate well the structural organization and mobility constraints of transmembrane segments in membrane proteins [3,51,52]. Moreover, the transmembrane peptide organization within the bilayer permits to establish more permanent interactions of the amino acids such as tyrosine with the regions of the membrane phospholipids that are oxidizable (*i.e.* allylic hydrogen of the carbon atom flanked by double bonds in unsaturated fatty acids). We mainly used as a prototypical oxidizing and nitrating species peroxynitrite, the product of the reaction of superoxide radicals and nitric oxide, which is a biologically-relevant oxidant and a known inductor of lipid peroxidation and tyrosine nitration [3]. Indeed, peroxynitrite can initiate free radical-dependent processes after its homolysis to •OH and $\bullet NO_2$ [1,3]. In the case of unsaturated fatty acids, they readily react with •OH ($k = 1 \times 10^{10}\ M^{-1}\ s^{-1}$) [53] and to a lesser extent with $\bullet NO_2$ ($k = 2 \times 10^{5}\ M^{-1}\ s^{-1}$ for linoleate at pH 9.4) [7], both of which promote hydrogen abstraction from a *bis*-allylic hydrogen to initiate an oxygen-dependent radical chain reaction with the formation of lipid-derived radicals. Lipid-derived radicals could oxidize other unsaturated fatty acids or other membrane components (including tyrosine residues) and yield lipid hydroperoxides. The "radical mix" of •OH, $\bullet NO_2$ and lipid-derived radicals, in turn, may promote tyrosine oxidation and nitration to yield products such as 3-hydroxytyrosine, 3,3′-dityrosine and, most notably, 3-NT. As a key reactant in the lipid peroxidation process, we purposely investigated the influence of molecular oxygen in tyrosine oxidation yields. The complexity of the oxidation process under study with several parallel, sequential and competing reactions plus the diffusional restrictions and spatial constraints of some of the key reactants demands the combination of approaches to obtain sound mechanistic insights. In particular, rationalization of observed tyrosine-peptide oxidation yields requires kinetic and molecular dynamics analysis. This work integrates experimental and computational evidence to support an intertwined mechanism of free radical-dependent lipid and protein oxidation in hydrophobic bio-structures.

1.1. Experimental procedures

1.1.1. Chemicals

Diethylentriaminepentaacetic acid (DTPA), manganese dioxide, sodium bicarbonate, sodium phosphate, potassium phosphate, L-tyrosine, 3-nitrotyrosine, α-tocopherol, γ-tocopherol, 1,1,3,3 tetra methoxypropane and hemin were purchased from SIGMA.

N-*t*-BOC L-tyrosine *tert* butyl ester (BTBE), 3-nitro- *N*-*t*-BOC L-tyrosine *tert* butyl ester (3-nitro-BTBE) and 3,3′ di-*N*-*t*-BOC L-tyrosine *tert* butyl ester (3,3′-di-BTBE) were prepared and handled as previously [9,48,49]. Stock BTBE solutions (1 M) were prepared in methanol immediately before use.

Transmembrane peptides Y4, Y8 and Y12 were from Bachem (reported purity: Y4: >87%, Y8: >90%, Y12: >89%) and have the following sequence:

Y4	Ac-NH-KKAYALALALALALALALAKK-CONH2 2350 Da
Y8	Ac-NH-KKALALAYALALALALALALAKK-CONH2 2350 Da
Y12	Ac-NH-KKALALALALAYALALALALAKK-CONH2 2350 Da

Peptide solutions were prepared dissolving peptide in methanol, or alternatively in methanol: TFA 2.5% and kept until use at −20 °C.

1,2-dilauroyl-*sn*-glycero-3-phosphocholine (DLPC) and egg yolk phosphatidylcholine (EYPC) were from Avanti Polar Lipids. Organic solvents for synthesis of standards and chromatography were from Baker or Mallinckrodt. All other compounds were reagent grade.

Peroxynitrite was synthesized as described below [54]. Stock hemin solution was freshly prepared in 0.1 N NaOH and kept in the dark at 4 °C until use. ABAP (2,2′-Azobis (2-amidinopropane) hydrochloride) was purchased from Wako Chemicals USA. A freshly stock solution (100 mM) was prepared in water immediately before used.

Argon and nitrogen gas were purchased in AGA Chemical Co. (Uruguay). All solutions were prepared with highly pure de-ionized nanopure water to minimize trace metal contamination.

1.1.2. Peroxynitrite synthesis and quantitation

Peroxynitrite was synthesized in a quenched-flow reactor from sodium nitrite ($NaNO_2$) and hydrogen peroxide (H_2O_2) under acidic conditions as described previously [54]. The H_2O_2 remaining from the synthesis was eliminated by treating the stock solutions of peroxynitrite with granular manganese dioxide, and the alkaline peroxynitrite stock solution was kept at −20 °C until use. Peroxynitrite concentrations were determined spectrophotometrically at 302 nm ($\varepsilon = 1670\ M^{-1}\ cm^{-1}$) [54,55]. The concentration of nitrite in the preparations was typically less than 20% respect to peroxynitrite. Control of nitrite levels revealed to be critical for obtaining reproducible data as, if present in excess; it can react with $^{\bullet}OH$ and other oxidants and yield $^{\bullet}NO_2$ [9,48]. In control experiments, peroxynitrite was allowed to decompose to nitrate in 100 mM phosphate buffer, pH 7.4 before use, *i.e.*, "reverse order addition" of peroxynitrite.

1.1.3. Tyrosine-probe incorporation into liposomes and oxidizing systems

BTBE or transmembrane peptide incorporation into liposomes was carried out as in Refs. [9,48–50] with minor modifications. Briefly, a methanolic solution of BTBE or transmembrane peptide (0.35 mM) was added to 35 mM PC lipids dissolved in chloroform, in order to achieve a final concentration of 0.3 mM tyrosine-probe and 30 mM lipid. The mixture was then dried under a stream of nitrogen gas. Multilamellar liposomes were formed by thoroughly mixing the dried lipid with 100 mM sodium phosphate buffer (pH 7.4) plus 0.1 mM DTPA. Previous studies from our group [9,48] already indicated that BTBE incorporation yields and formation of oxidation products from peroxynitrite were comparable in unilamellar and multilamellar liposomes and therefore not noticeably dependent on the membrane morphology. Therefore, due to the simpler and more efficient preparation procedure, reported experiments were carried out mainly with multilamellar liposomes. Importantly, some key experiments were also performed in unilamellar liposomes, which were prepared as in Ref. [56] with minor modifications. Specifically, unilamellar liposomes were obtained by sonication of the ice-chilled lipid suspension in buffer with a probe sonicator (60 W, three cycles of 30 s) until the suspension became clear. Samples were centrifuged for 10 min at 8000 g to remove metal particles and any remaining multilamellar liposomes.

For experiments with α/γ-tocopherol-containing liposomes, α/γ-tocopherol (in ethanol) was added at the desired concentration to the lipid solution in chloroform with or without tyrosine probe and liposomes prepared thereafter as indicated above. Liposomes were exposed to peroxynitrite, hemin or ABAP under different conditions throughout the work.

BTBE and BTBE-derived products (*e.g.* 3-nitro-BTBE and 3,3′-di-BTBE) were extracted with chloroform, methanol and 5 M NaCl as reported previously (1:2:4:0.4, sample: methanol: chloroform: NaCl v/v with recovery efficiencies for all compounds > 95% [49]). Samples were then dried and stored at −20 °C. Immediately before HPLC separation, samples were resuspended in 100 μl of a mixture containing 85% methanol and 15% KPi (15 mM) pH 3.

Liposomes with incorporated peptides were exposed to desired concentrations of peroxynitrite, hemin or ABAP in a final volume of 100 μl. The reaction was diluted with 1900 μl distilled water and centrifuged at 12800 rpm at 4° C for 120 or 240 min for multilamellar or unilamellar liposomes, respectively; the pelleted liposomes were dried by a vacuum evaporator (Speedvac SOD1010P1 Thermo Scientific) or under a stream of argon. The dried liposome was dissolved in 100 μl of methanol containing 2.5% of trifluoroacetic acid and HPLC analysis were carried within the next 12 h. In all tested conditions, addition of decomposed-peroxynitrite (reverse order addition) gave no detectable nitration products.

In some experiments, peroxynitrite addition was performed in the presence of sodium bicarbonate (25 mM) in buffer KPi (100 mM) plus DTPA (0.1 mM), pH 7.4. The final pH of the buffer was controlled after the addition of bicarbonate.

Experiments with liposomes were performed at room temperature (25 °C), a temperature above the transition phase temperatures of the different liposomes and at 37 °C when ABAP was used as an oxidant.

1.1.4. Oxidation systems

BTBE or transmembrane peptide-containing PC liposomes were oxidized either by the addition of peroxynitrite, hemin or the organic peroxyl radical donor ABAP. Peroxynitrite was added as a single bolus under vigorous vortexing ($t_{1/2} = 2.5$ s at 25 °C [57]) or by slow infusion using a motor-driven syringe system (Kd Scientific) under continuous stirring. Due to the addition of alkaline peroxynitrite solutions, the final pH was systematically checked at the end of the incubations to make sure that there were no significant variations (<0.1 pH units) and the final pH was recorded. Hemin was added directly to the PC liposomes; EYPC liposomes always contain a basal level of pre-formed lipid hydroperoxides that serve as the redox substrate for hemin (25 μM). Alternatively, *tert*-butyl hydroperoxide was used as hemin reactant in DLPC liposomes. Finally, in the case of ABAP, samples were incubated at 37 °C during 2 h to achieve a final ABAP concentration of 20 mM with or without 40 mM $NaNO_2$. ABAP-dependent oxygen consumption was measured using a high-resolution oxymeter (Oroboros 2K) yielding a flux of 0.3 μM/min of $LOO^{\bullet}$ radicals.

1.1.5. Lipid peroxidation analysis

Analysis of malondialdehyde (MDA), a byproduct of lipid peroxidation, was performed after its reaction with thiobarbituric acid

by UV/Vis (λ at 532 nm, $\varepsilon = 150{,}000\ M^{-1}cm^{-1}$) and/or fluorimetric detection [55]. Calibration curves and assessment of malondialdehyde content were performed with known amounts of MDA obtained from the acid hydrolysis of 1,1,3,3 tetramethoxypropane in 20% acetic acid pH 3.5. To prevent further peroxidation of lipids during assay procedures, 0.05% (w/v) of butylated hydroxytoluene (BHT) was added to the TBARS reagent. Alternatively, the formation of lipid hydroperoxides was assessed by the ferrous oxidation-xylenol orange assay (FOX) as described previously [58]. Indeed, lipid hydroperoxides were measured spectrophotometrically by the oxidation of Fe^{2+} in the presence of xylenol orange in an acidic environment. The liposome sample was mixed with the FOX reagent (100 mM xylenol orange; 250 mM ferrous ammonium sulfate (source of Fe^{2+}); 25 mM H_2SO_4; and 4 mM BHT in 90% (v/v) methanol). Reaction mixtures were incubated for 1 h at room temperature, and the absorbance of the xylenol orange-Fe^{3+} complex was measured at 560 nm ($\varepsilon_{XO\text{-}Fe3+} = 43{,}000\ M^{-1}\ cm^{-1}$), as described previously [9,59].

1.1.6. HPLC analysis

BTBE, 3-nitro-BTBE and 3,3′-di-BTBE were separated on a Agilent 1200 system equipped with UV-Vis and fluorescence detectors by reverse-phase HPLC using an Agilent Eclipse XDB-C18 5 μm column (150 mm length, 4.6 mm ID) as reported previously [9,48]. Mobile phase A consisted in 15 mM phosphate buffer pH 3 and mobile phase B consisted in methanol. Chromatographic conditions were: flow 1 ml/min; 75% mobile phase B for 25 min, followed by a linear increase to 100% mobile phase B for 10 min. UV-Vis settings were for BTBE (280 nm, $\varepsilon = 1200\ M^{-1}cm^{-1}$) and for 3-nitro-BTBE (360 nm, $\varepsilon = 1500\ M^{-1}cm^{-1}$). 3,3′-di-BTBE was detected fluorimetrically at $\lambda_{ex} = 294$ nm, $\lambda_{em} = 401$ nm. Authentic 3-nitro-BTBE and 3,3′-di-BTBE were used as standards.

3-Nitrotyrosine and 3,3′-dityrosine were separated by reverse-phase HPLC, using a Partisil ODS-3 10 μm (250 mm length, 4.6 mm ID) C18 column as previously reported with minor modifications [9,48]. Briefly, separation of tyrosine oxidation products was performed by isocratic RP-HPLC. Chromatographic conditions were: flow 1 ml/min; 97% mobile phase A (KPi 15 mM pH 3) and 3% mobile phase B (methanol) for 30 min 3-Nitrotyrosine was measured by UV detection (280 nm and 360 nm) and 3,3′-dityrosine was measured fluorometrically ($\lambda_{ex} = 280$ nm and $\lambda_{em} = 400$ nm). Authentic 3,3′-dityrosine and 3-nitro-Tyr were used as standards.

Transmembrane nitration Y4, Y8 and Y12 products were separated by RP-HPLC using the following gradient in an Agilent Eclipse XDB-C18 5 μm column (150 mm length, 4.6 mm ID). Chromatographic conditions were: flow 0,75 ml/min; time 0: 40% mobile phase A (Water-TFA 0.1%) and 60% mobile phase B (acetonitrile). Time 25 min: 85% mobile phase A and 15% mobile phase B. Time 32 min: 40% mobile phase A and 60% mobile phase B. Nitration products were measured by UV/Vis detection at 280 and 360 nm. Calibration curves were prepared by using authentic 3-nitro-peptides as standards as described previously [50]. Nitropeptides showed the characteristic UV-Vis spectrum. After adding NaOH, the 350 nm absorption peak in MeOH was shifted to 430 nm with an extinction coefficient of 4100 $M^{-1}cm^{-1}$. The formation of transmembrane peptide dityrosine was followed fluorimetrically ($\lambda_{ex} = 294$ nm and $\lambda_{em} = 401$ nm).

Artifactual tyrosine nitration during the chromatographic separation procedures due to nitrite-dependent nitration at acidic pH, were ruled out in all model systems (*i.e.* free tyrosine, BTBE, tyrosine peptides) by appropriate controls using pre-decomposed peroxynitrite (reverse order addition experiments).

In all the experimental conditions, tyrosine nitration and lipid peroxidation levels were evaluated in the absence of oxidant. While nitrated peptide was never detectable in the control condition, basal levels of pre-formed lipid hydroperoxides and MDA were detected in EYPC liposomes as indicated in the corresponding figure legends.

1.1.7. Oxygen-controlled experiments

Experiments under different oxygen concentrations (1–21% in the gas phase) were performed in a hypoxic chamber (CoyLab Instruments). For the oxygen-controlled reactions, samples were prepared as indicated above, but peroxynitrite addition was performed inside the chamber at controlled oxygen levels of 1–21% which result in concentrations of 10–210 μM O_2 in solution in the utilized buffer systems at room temperature. The hypoxic chamber was equilibrated for 30 min in each condition with the samples prior to the addition of peroxynitrite. Some experiments were also performed in argon-saturated solutions to reach oxygen levels $\leq$1%.

1.1.8. Kinetic simulations

Computer-assisted kinetic simulations were performed to assess yields of 3-NT in the presence of peroxynitrite added either as a bolus or slow infusion. Time course of reactants (peroxynitrite, molecular oxygen) and intermediates (tyrosyl and lipid peroxyl radicals) in the process were also analyzed. We also studied the influence of molecular oxygen and α-tocopherol on the extent of 3-NT formation. *In silico* reactions were performed with the software Gepasi (version 3.3) [60,61], as in previous works from our group [9,45,48,62,63]. The kinetic simulation studies utilized in most cases available rate constant values previously obtained in aqueous solution, yet applied to a diffusion-restricted system. Thus, when possible, diffusion restriction events and partitioning effects were considered for these studies.

1.2. Molecular dynamics simulations

To build the final membrane-tyrosine peptide system, we used a three step *in silico* protocol. In the first place, we built a palmitoyl-2 linoleoyl-sn-glycero-3 phosphatidylcholine (PLPC) hydrated bilayer, taking as the starting point an equilibrated palmitoyl-2 oleoyl-sn-glycero-3 phosphatidylcholine (POPC) hydrated bilayer obtained from Klauda et al. [64], and performing the required changes in molecular structure *in silico*. The resulting system consisted in 72 PLPC and 2242 water molecules. The system was subject to a minimization procedure of 1000 steps, followed by a 2 ns long MD simulation in the NPT ensemble with reference pressure and temperature values of 300 K and 1.013 bar, respectively. During this stage, a 2 fs time-step was used to integrate the Verlet equation using the NAMD code [65]. After equilibration, a 50 ns long MD simulation was performed restricting the XY planar box area at a value of 70 $Å^2$/PLPC. For the production runs, we employed an hydrogen mass repartitioning scheme, that allows increasing the integration time-step to 4 fs, [66]. The average orientation of the hydrophobic chains and of the P-N vector with respect to the bilayer surface was 90, and 0°, respectively, consistently with experimental results.

The second step, corresponds to the building of the peptide-membrane model. For this sake, three PLPC molecules from each side of the equilibrated bilayer were removed, and in their place we inserted the Ac-NH-KKALALALALALALALALAKK-$CONH_2$ peptide in an alpha helix conformation. The system was neutralized with 4 chloride anions, and subject to a minimization process followed by a 2 ns long MD equilibration, using a 2 fs time-step. Harmonic constraints were applied for all peptide atoms. Finally, a 50 ns long MD simulations were performed without any restraint and using a 4 fs time-step.

Finally, the third and final step required to obtain the Tyr containing peptides, consisted in *in silico* mutating of either Leu 4, Leu

8 or Leu 12 to Tyr. Once built, each of the three systems was subject to minimization, followed by 100 ns of production MD simulations using a 4 fs time-step.

All MD simulations were performed using the CHARMM36 FF force field [64] for lipids and amino acids and the TIP3P water model, with a cutoff of 9 Å, a smooth switching function of 7.5 Å and a non-bonded pair list set of 9.5 Å. Long-range electrostatic interactions were computed using the particle-mesh Ewald method with the grid spacing of 1 Å [67].

1.2.1. General experimental conditions

Experiments were typically carried out in the presence of BTBE or peptide (0.3 mM) in PC liposomes (30 mM) in 100 mM potassium phosphate plus 0.1 mM DTPA (pH 7.4) and room temperature (23-25 °C), unless otherwise stated. For the MDA determinations, sodium phosphate buffer was used to avoid interference with the detection method.

1.2.2. Data analysis

All experiments reported herein were repeated at least three times and results are expressed as mean values with the corresponding standard deviations, of at least three experimental determinations. Graphics and data analysis were performed using GraphPad Prism version 5.0b. Statistical analysis of the data presented was analyzed by ANOVA followed by Tukey's Multiple Comparison Test ($p < 0.05$).

2. Results

2.1. Peroxynitrite-mediated peptide nitration and lipid peroxidation

Previous results of our group using the hydrophobic tyrosyl-probe BTBE showed the existence of a connecting reaction between lipid peroxidation and nitration reactions in membranes, by which lipid-derived radicals formed during lipid peroxidation, (*i.e.* LOO• and LO•) can promote the one-electron oxidation of tyrosine within the membrane yielding Tyr•, which in the presence of $•NO_2$ can lead to the formation of 3-NT, among other tyrosine oxidation products [9]. In the present work, we have extended the initial observations to a more biologically-relevant model system, using tyrosine-containing transmembrane spanning peptides [50] incorporated to liposomes, and compared with data obtained both with BTBE (in membranes) and tyrosine (in aqueous solution).

These peptides have been extensively used as transmembrane protein models, since their structure resemble the transmembrane segments of these proteins [51]. There are several variants of these peptides. Herein, we used KALP peptides, consisting in α-helical arrangements formed by a hydrophobic core consisting in the alternation of hydrophobic amino acids such as Ala-Leu, flanked by charged amino acids such as Lys, interacting with the interphase, which anchor the peptides to the bilayer.

The basic membrane model composition and structural assembly is shown in Fig. 1.

The three transmembrane peptides Y4, Y8 and Y12 were incorporated to phosphatidylcholine liposomes of different fatty acid composition, namely, saturated (DLPC) and unsaturated (EYPC), and exposed to peroxynitrite.

It is important to note that DLPC consists in saturated lauryl acid (12:0), while EYPC contains a mixture of saturated and unsaturated fatty acids, with a total percentage of polyunsaturated fatty acids of 20.7%, being the most abundant linoleic acid (18:2) [68].

Nitration yields were dependent on peroxynitrite concentration in a dose-dependent manner, especially in unsaturated liposomes, either when peroxynitrite was added as a bolus (Fig. 2, Panel A) or as a slow infusion (Fig. 2 Panel B). Nitration yields, defined as molar percentage of 3-nitrotyrosine/peroxynitrite, were determined on the linear portion of the curve, *e.g.* at 500 μM peroxynitrite. In DLPC, tyrosine nitration yields were *ca.* 3% respect to added bolus peroxynitrite for all three peptides (Fig. 2, Panel A) (Table 1). In agreement with results obtained previously with the hydrophobic tyrosine analog BTBE [9] nitration yields were higher for unsaturated liposomes, supporting a participation of lipid radicals in tyrosine oxidation. Nitration yields of Y8 and Y12 were consistently higher than those observed for Y4, in all tested systems, suggesting that nitration of tyrosine residues more deeply located in the bilayer is favored. No 3,3′-dityrosine-containing peptide was detected in our experimental conditions. Selected experiments performed with Y8-containing unilamellar liposomes showed that peroxynitrite-mediated nitration yields and lipid hydroperoxides levels were comparable to those obtained with multillamelar liposomes (data not shown).

Nitration yields by peroxynitrite in Y8 were also evaluated in the presence of 25 mM sodium bicarbonate; under this condition peptide nitration was inhibited (*ca.* 40% and 47% inhibition in DLPC and EYPC, respectively), similarly to previous results on BTBE nitration in liposomes [9,48]. Likewise, lipid hydroperoxide formation in unsaturated liposomes, was also inhibited (*ca.* 25%) in the presence of bicarbonate.

The comparison of probe oxidation yield in the presence of bolus or infusion of peroxynitrite is worth to analyze (Table 1). Peroxynitrite has a half-life of 2.5 s in 100 mM KPi buffer, pH 7.4 and 25 °C. Although it is more practical from an experimental point of view, the addition of peroxynitrite as a single bolus results in a high initial concentration of radicals which favor termination reactions. Moreover, this situation may not reflect biologically-relevant conditions in which peroxynitrite is formed as a continuous flow [69]. Interestingly, nitration yields from peroxynitrite added as a slow infusion were consistently higher than those of bolus addition (Fig. 2, Panel B).

Due to the important amount of unsaturated lipids present in EYPC liposomes, we also evaluated the formation of lipid hydroperoxides in the presence of peroxynitrite added either as a bolus (Fig. 2, Panel C, left), or a slow infusion (Fig. 2, Panel C, right). As expected, no lipid hydroperoxides were detected in the saturated DLPC liposomes (data not shown); however, in the unsaturated liposomes lipid hydroperoxides were measured in all three peptide-containing liposomes. The levels of lipid hydroperoxides were higher than those of nitrated peptide, consistent with the larger abundance of the unsaturated fatty acid *vs.* the tyrosine analog present in the liposomes and due to the propagative nature of the lipid peroxidation process (see also later, Fig. 6).

Table 1 shows a side-by-side comparative analysis of tyrosine nitration yields for free tyrosine, BTBE and Y8, for both bolus addition and infusion of peroxynitrite. Nitration yields were in the order tyrosine > BTBE ≈ Y8. The lower nitration yields of the hydrophobic-tyrosyl probes, in comparison with free tyrosine is consistent with our previous report [9]. In the case of free tyrosine, the data recapitulate previous observations on nitration yields being higher for bolus addition than for infusion [70]. On the contrary, the nitration of the hydrophobic tyrosine analog Y8, was higher with peroxynitrite infusion in agreement with the previous [9] and present data (Table 1) on BTBE, underscoring differences on the chemistry of the tyrosine oxidation process in membranes *vs* that in aqueous solution (see also Discussion).

2.2. Hemin and ABAP-mediated peptide nitration and lipid peroxidation

We have previously demonstrated that lipid peroxyl [9] and alkoxyl radicals [10] can promote the one-electron oxidation of

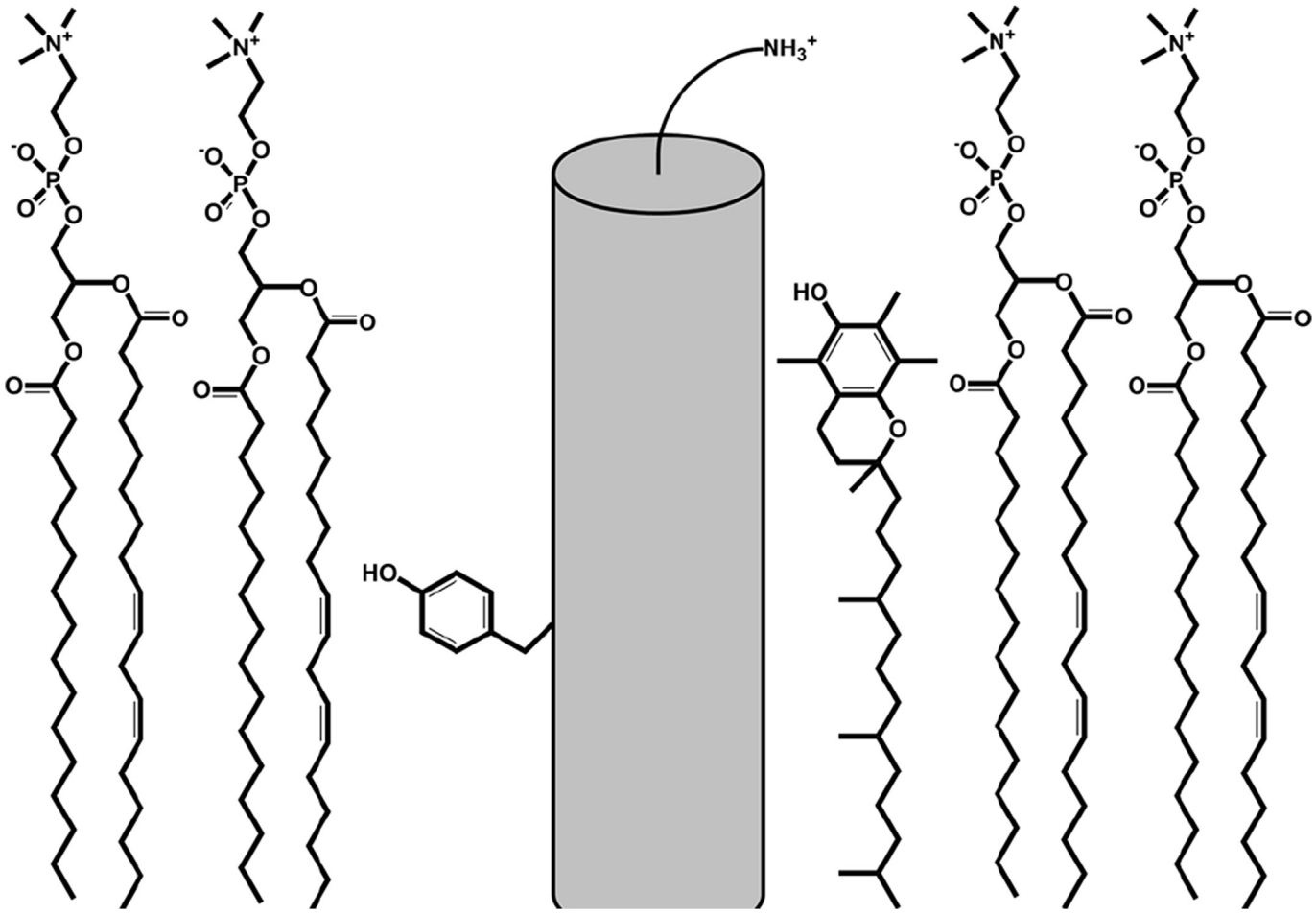

Fig. 1. Basic membrane model system. The model consists in PC liposomes (unsaturated 18:2 fatty acids) with pre-incorporated membrane-spanning tyrosine peptides. A membrane monolayer is drawn for the sake of simplicity and the tyrosine peptide schematically represents Y8, which is approximately halfway immersed into the monolayer. The phenol group in Y8 is adjacent to the double bonds of linoleic acid (see text). The model also shows in the right of Y8 the presence of the chain-breaking antioxidant α-tocopherol with the chromanol ring facing the lipid-water interphase and the 12-carbon aliphatic side chain entering deep into the membrane.

tyrosine leading to the formation of Tyr•, potentially fueling by this way the tyrosine oxidation and nitration pathways in membranes.

To further assess the role that lipid peroxidation processes may play in membrane tyrosine nitration, DLPC and EYPC peptide-containing liposomes were exposed to ABAP and hemin both of which efficiently lead to the formation of LOO• in unsaturated fatty acid-containing membranes. On one hand, ABAP is an organic peroxyl radical-donor, which initiates oxidation by the generation of ROO• (peroxyl radicals) by thermolysis, which in turn initiate lipid peroxidation. On the other hand, free hemin interacts with membranes [71] and triggers lipid peroxidation by the reaction with pre-formed lipid hydroperoxides (LOOH) normally present in unsaturated fatty acid-containing liposomes preparations. Hemin-(Fe^{3+}) promotes the one-electron oxidation of LOOH, yielding LOO• and hemin- (Fe^{2+}); in turn, hemin- (Fe^{2+}) can generate LO• by reduction of LOOH [9]. As expected, in the presence of ABAP alone, no nitrated tyrosine peptide was detected. When the ABAP reaction was further supplemented with nitrite (NO_2^-), 3-NT was detected in both, saturated and unsaturated liposomes (Fig. 3A). Similar results were obtained in the presence of hemin (Fig. 3A). These results confirm that tyrosine residues are being oxidized by LOO• formed from either ABAP or hemin in EYPC, and that in the presence of nitrite, nitrating species were also generated (*i.e.* $•NO_2$) to yield the tyrosine nitrated peptide (in the case of DLPC, nitration of the peptide occurs by the direct reaction of ABAP-derived peroxyl radicals with both tyrosine and nitrite). Of note, LOO• are capable of promoting the one-electron oxidation of nitrite to $•NO_2$ needed for the reaction with Tyr• to form 3-NT [72].

In both systems, lipid hydroperoxide formation was evaluated. As expected, no lipid hydroperoxides were detected in saturated DLPC liposomes, while they were significantly formed in unsaturated liposomes. The amount of LOOH detected (*ca.* 380 μM and 360 μM for ABAP) was similar in the presence or absence of nitrite (Fig. 3B).

2.3. Peptide nitration in membranes: influence of molecular oxygen

Oxygen is a critical reagent in the formation of lipid LOO • radicals and, in consequence, in the propagation phase of lipid peroxidation. Thus, if transmembrane-peptide tyrosine nitration is connected to lipid peroxidation, oxygen levels should influence peptide oxidation yields. To perform these experiments in a controlled-manner, we used a hypoxic chamber in which a range of dissolved oxygen concentrations (*i.e.* solutions equilibrated at 2–21% oxygen) in the reaction system can be tested.

Nitration yields for the three peptides increased at higher oxygen concentration (5 and 21%) for both DLPC and EYPC liposomes, with the effect more remarkable in unsaturated fatty-acid containing EYPC liposomes (Fig. 4A). Importantly, in EYPC liposomes Y8 and Y12 nitration yields were consistently higher than Y4. In

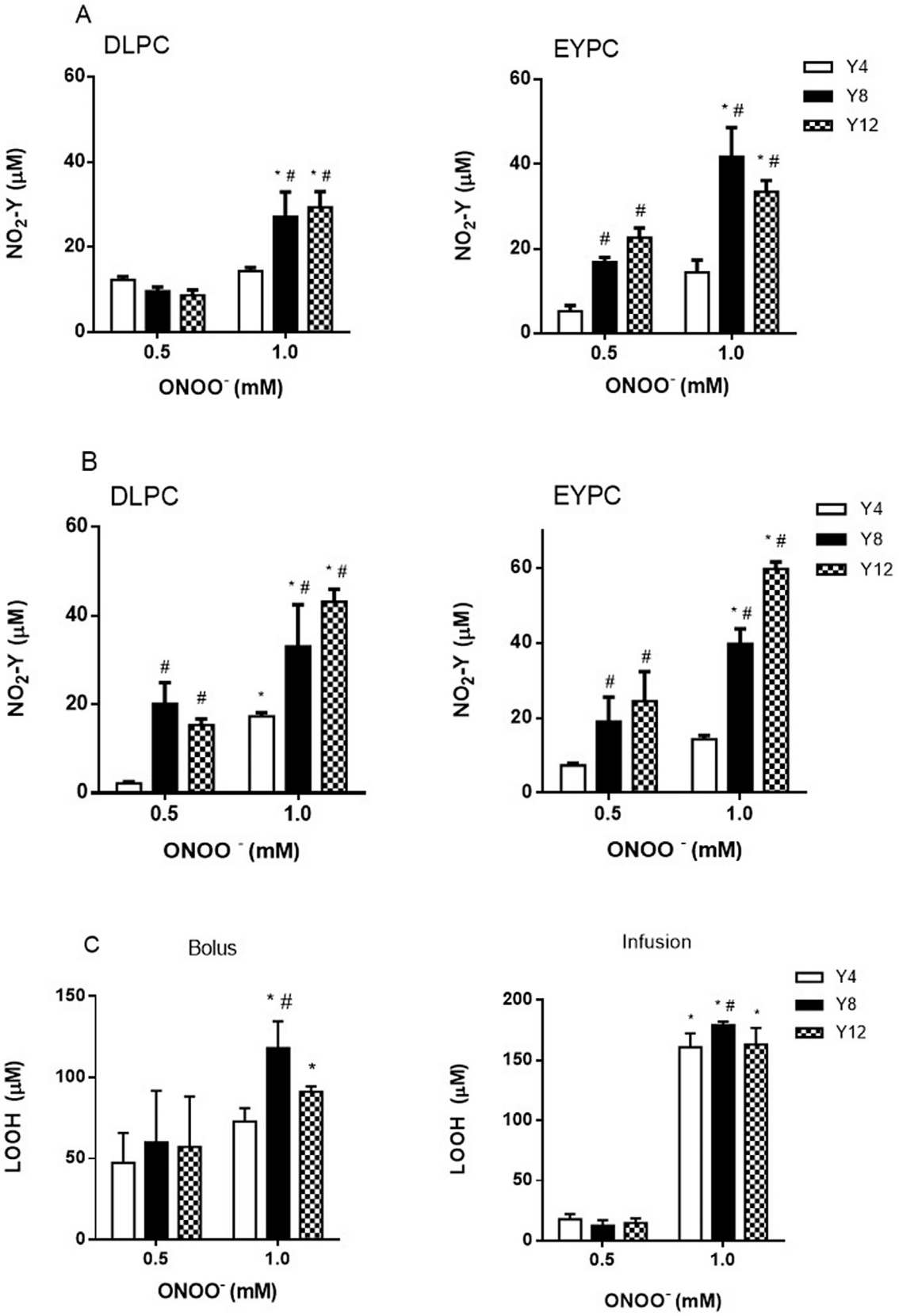

Fig. 2. Peroxynitrite-dependent peptide nitration: Bolus *vs* slow infusion addition. Peptides Y4, Y8 and Y12 (0.3 mM), were incorporated to DLPC (saturated) and EYPC (unsaturated) (30 mM) in KPi 100 mM pH 7.3 + 0.1 mM DTPA liposomes, and exposed to peroxynitrite (0–1 mM) added as a single bolus **(Panel A)** or as a slow infusion (50 μM/min) at room temperature **(Panel B).** The formation of 3-nitropeptide was analyzed by UV/Vis detection after RP-HPLC. In addition, lipid peroxidation was studied through the formation of hydroperoxides by FOX assay when peroxynitrite was added as a bolus or slow infusion in EYPC liposomes **(Panel C).** Pre-formed lipid hydroperoxides and MDA were detected in control EYPC liposomes (13 ± 2 μM and 2.5 ± 1, respectively), and all data shown illustrate the increase over the control condition. Symbols above the bars denote statistical differences for the condition of 1.0 mM compared to 0.5 mM $ONOO^-$ for each peptide (*) and for Y8 and Y12 compared to Y4 at the same concentration of $ONOO^-$ (#), using the Tukey's multiple comparison test ($p < 0.05$).

Table 1
Comparative analysis of tyrosine nitration yields.

Liposome	Y	$ONOO^-$ (bolus)			$ONOO^-$ (Infusion)		
–	Tyr	NO_2-Y (μM)	Di-Y (μM)	NO_2-Y (%)[a]	NO_2-Y (μM)	Di-Y (μM)	NO_2-Y (%)
		42.41 ± 3.23	8.06 ± 0.08	8.5	31.58 ± 1.16	19.31 ± 3.04	6.3
DLPC	BTBE	12.95 ± 1.20	0.25	2.60	30.3 ± 5.79	0.07	6.06
DLPC	Y8	14.55 ± 3.17	0	2.91	23.52 ± 3.13	0	4.70

Nitration yields of the different tyrosine-containing peptides, BTBE and free tyrosine after bolus (0.5 mM) or slow infusion (25 μM/min for 20 min) addition of peroxynitrite.
[a] Nitration yield is related to added concentration of peroxynitrite (500 μM).

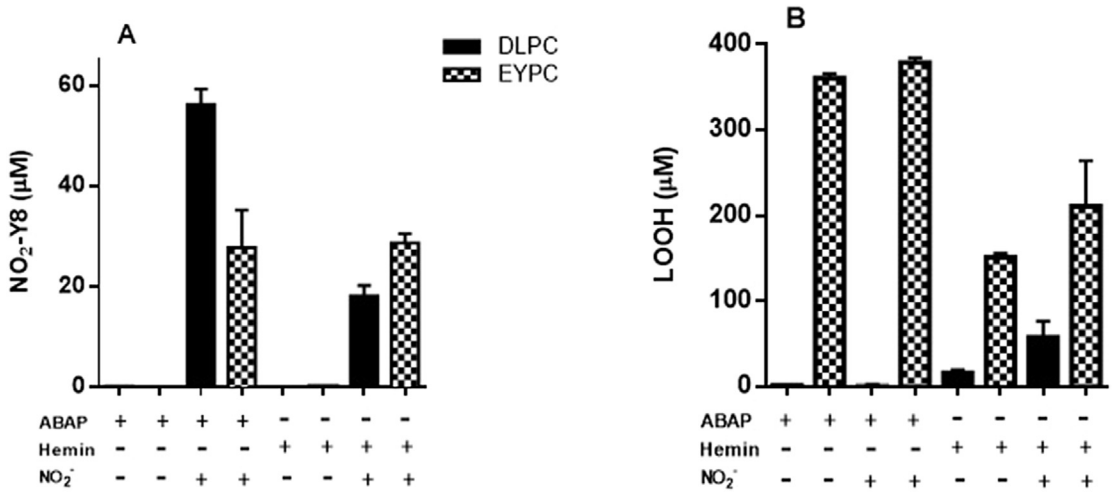

Fig. 3. Hemin and ABAP-mediated peptide nitration and lipid peroxidation. Peptide Y8 (0.3 mM), was incorporated to DLPC and EYPC (30 mM) liposomes in KPi 100 mM pH 7.3 + 0.1 mM DTPA, and exposed to ABAP (20 mM) +/− $NaNO_2$ (40 mM) or to hemin (25 μM) +/− $NaNO_2$ (40 mM) The formation of 3-nitropeptide was analyzed by UV/Vis detection after RP-HPLC **(A)**. Lipid hydroperoxides were determined by FOX assay **(B)**.

agreement with the role of oxygen in the propagation of lipid peroxidation, MDA levels in the different EYPC liposomes also increased at higher oxygen tensions (Fig. 4B).

Furthermore, the nitration of peptide Y8 was evaluated on a broad range of oxygen concentrations (1–21% O_2); as shown in Fig. 4C, nitration yields were highly dependent on oxygen concentration, being the effect more pronounced in the unsaturated EYPC liposomes. In addition, MDA yields in EYPC unsaturated liposomes increased as a function of oxygen concentration; no MDA was detected in the saturated DLPC ones throughout the oxygen concentration range (Fig. 4D).

To further demonstrate the point that the influence of molecular oxygen is related to the modulation of lipid LOO• radical formation, additional parallel experiments were performed with the hydrophobic tyrosine analog BTBE incorporated to PC liposomes and free tyrosine in solution (Fig. 4E). The experiments clearly show that when the tyrosine moiety is incorporated to the lipidic structure, BTBE nitration yields increased as a function of oxygen concentration, notably in EYPC liposomes. Conversely, there was absolutely no influence of oxygen concentration on peroxynitrite-dependent tyrosine nitration for free tyrosine in solution as nitration yields remained constant throughout the oxygen concentration range (Fig. 4F).

2.4. Modulation of transmembrane peptide tyrosine nitration by α-tocopherol

α-Tocopherol is a well-known lipophilic antioxidant that reacts with LOO• with a rate constant of $1 \times 10^8\ M^{-1}\ s^{-1}$ [73] and therefore inhibits the propagation phase of the lipid peroxidation process. In turn, γ-tocoperol in addition to react with LOO• (although with somewhat less efficiency), is also able to trap •NO_2 [74].

Alpha -and γ-tocopherol incorporated into EYPC liposomes inhibited in parallel, peroxynitrite-mediated tyrosine peptide nitration (shown in Fig. 5A for α-tocopherol) and lipid peroxidation in a dose-dependent manner.

At 0.5 mM peroxynitrite, the inhibitory effect became evident at α-tocopherol *ca.* 50 μM, which is consistent with the amounts of radical species formed upon peroxynitrite decomposition (30% homolysis [75–77]) and a stoichiometric factor n = 2 for the reactions of α-tocopherol with one-electron oxidants. For example, according to the FOX assay (Fig. 2C) and by MDA determination (Fig. 5B) (*ca.* 5% yield of MDA from decomposing LOOH [9]) 0.5 mM bolus peroxynitrite resulted in the formation of *ca.* 50 μM and 20 μM of lipid hydroperoxides and nitrated Y8, respectively. 50 μM α-tocopherol decreased the oxidation products in the range of 30–50% in good agreement with a connecting process between lipid peroxidation and peptide nitration. Interestingly, γ-tocopherol, also inhibited both processes in agreement with its capacity to react with LOO• and peroxynitrite-derived radicals such as •NO_2 [74] (data not shown).

α-tocopherol also inhibited peptide nitration in DLPC liposomes where no lipid peroxidation occurs. However, as •OH radicals derived from the homolysis of peroxynitrous acid react with the saturated fatty acids at fast rates ($6.4 \times 10^8\ M^1 s^1$ [78], still lipid peroxyl radicals will be formed. In the case of saturated lipids, the reaction of α -tocopherol with •NO_2 ($k = 1 \times 10^5\ M^{-1}\ s^{-1}$ [79]) also becomes relevant to explain the inhibition of tyrosine peptide oxidation and nitration.

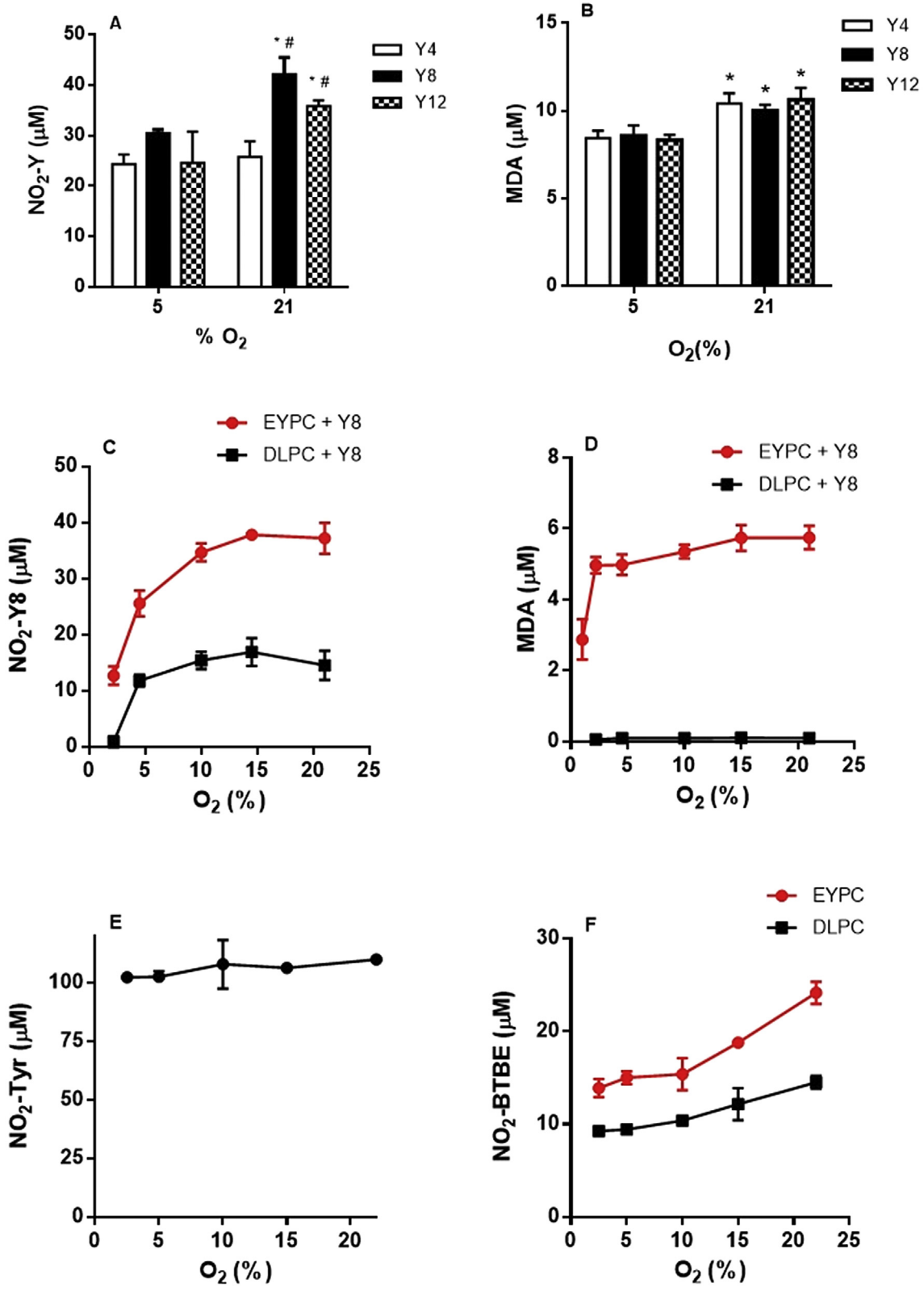

Fig. 4. Effect of oxygen on tyrosine nitration yields. Tyrosine-containing peptides (Y4, Y8 and Y12) were incorporated to liposomes (30 mM) in KPi 100 mM pH 7.3 + 0.1 mM DTPA and exposed to peroxynitrite (1 mM) at 25 °C at the indicated oxygen concentrations and 3-nitro-peptide **(A)** or MDA formation in EYPC was evaluated **(B).** Y8 nitration **(C)** and MDA formation **(D)** was evaluated in a broad range of oxygen concentrations (10–210 μM O_2) for EYPC and DLPC. Free tyrosine **(E)** or BTBE incorporated to liposomes **(F)** in KPi 100 mM pH 7.3 + 0.1 mM DTPA were exposed to peroxynitrite (1 mM) at different oxygen tensions. The formation of 3-nitro-peptide, 3-nitro-BTBE or 3-nitrotyrosine was analyzed by RP-HPLC. MDA formation was measured by an HPLC-based fluorimetric analysis. Symbols above the bars denote statistical differences for the condition of 21% compared to 5% for each peptide (*) and for Y8 and Y12 compared to Y12 and Y4 at the same concentration of O_2 (#), using the Tukey's multiple comparison test ($p < 0.05$).

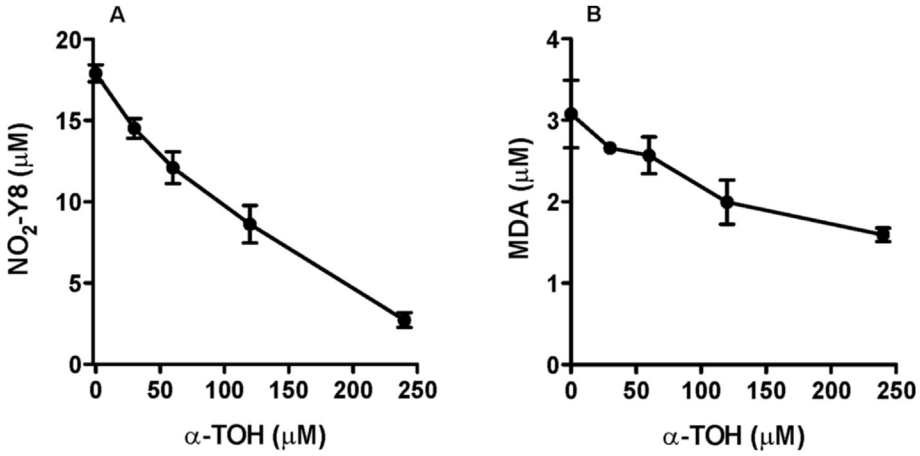

Fig. 5. Effect of α-tocopherol on peroxynitrite-mediated lipid peroxidation and peptide nitration. Y8 (0.3 mM) and the indicated concentrations of α-tocopherol (0–250 μM) were pre-incorporated to EYPC liposomes (30 mM) in KPi 100 mM pH 7.3 + 0.1 mM DTPA and treated with peroxynitrite (0.5 mM). Samples were analyzed for 3-nitro-Y8 **(A)** and MDA **(B)** contents.

2.5. Kinetic simulations studies on the lipid-tyrosine oxidation connection reaction

In order to get further evidence on the role that lipid peroxidation has in promoting tyrosine oxidation and how this process affects overall tyrosine nitration yields, we performed computer-assisted kinetic simulation studies considering all main known participating oxidation reactions during peroxynitrite addition to tyrosine-containing phosphatidylcholine liposomes. The main processes considered are shown in Table 2 and were peroxynitrite homolysis and dismutation (Eqs. (18)–(20) and (29), respectively), lipid peroxidation (Eqs. (1), (2), (8)–(14)) and tyrosine oxidation/nitration (Eqs. (3)–(7)). Additionally, studies were performed analyzing the effects of α-tocopherol (Eqs. (15)–(17)).

A first important observation is that, in agreement with the experimental data (Fig. 2), addition of peroxynitrite into the system as a flux resulted in higher levels of 3-nitropeptide than addition as bolus (Fig. 6A). This result contrasts with what is observed experimentally with free tyrosine [70] (and that can be also computationally-reproduced, Fig. S1, panel A Supporting Information) and has to do with the unique characteristics of tyrosine oxidation in the hydrophobic environment (see Discussion).

Notably, the kinetic simulation studies perfectly recapitulated the dependency of peptide tyrosine nitration yields as a function of oxygen concentration (Fig. 6B), underscoring the relevance of lipid peroxidation in fueling peroxynitrite-dependent tyrosine nitration. To note, in the simulations shown in Fig. 6 the concentration values used were those of the buffer solution, but a similar trend was observed if oxygen concentration values were tripled (Fig. S2, Supporting Information) considering that inside the membranes O_2 may be more concentrated (*i.e.* partition ratio of up to 3/1 respect to aqueous phase) [80].

Of note, during the lipid peroxidation process oxygen concentrations decrease (Fig. 6C, inset), but the chemistry involving the "connecting reaction" (Eq. (14)) continues to be a central process until very low oxygen levels are achieved at time *ca.* 2 s and as can be seen by the time course of lipid peroxyl radicals (Fig. 6C). Indeed, while the decay of peroxynitrite occurs over a *ca.* 10 s period (Fig. 6D), the formation of 3-nitrotyrosine substantially increases as a function of time until *ca.* 2 s, after which a significant decrease in rate and minor increment in yield is observed (Fig. 6D).

Finally, incorporation of α-tocopherol into the computational analysis resulted on inhibition of tyrosine nitration yields and lipid hydroperoxides (Fig. 6E and F), in agreement with the experimental results. However, we must note that the inhibitory effect of α-tocopherol was more significant in the actual experiments than in the simulations; while the reason for this minor discrepancy is not apparent and might depend on subtle variations in rate constant values, it further underscores the role of LOO• in promoting tyrosine nitration reactions.

In combination, the influence of molecular oxygen and α-tocopherol observed experimentally and computationally on peptide nitration yields provide further support for the kinetic model and the mechanistic proposal (Table 2) associating the lipid peroxidation with the tyrosine nitration processes in tyrosine peptide-containing membranes.

2.6. Molecular structural dynamics in transmembrane peptide-containing liposomal membranes

The membrane system is a highly organized biostructure and the proposed "connecting reaction" requires the interaction between the tyrosine phenolic oxygens (located at different positions in the membrane in Y4, Y8 and Y12) and the LOO• group, mainly formed at C9 and C13 of linoleic acid. Thus, we assessed the spatial relationship (position along the Z-axis) of the double bonds in the oxidizable fatty acids, relative to the position of the tyrosine phenolic oxygen in each peptide by performing MD simulations of the corresponding systems.

A typical snapshot of the molecular dynamics simulation of the peptide Y8 inserted in the bilayer is shown in Fig. 7. In all cases, the membrane with the inserted peptides turned out to be stable during the time scale of the simulation, with both the hydrocarbon chains and P-N vector orientations similar to those observed in the pure membrane case.

In order to analyze the structural fluctuations of the Tyr residues, which may be related to their chemical reactivity with peroxyl radicals generated at C9 and C13, we have monitored the time evolution of the phenolic O, and the C9, and C13 of the hydrocarbon chains distance to the bilayer center. As controls, we have also monitored the P and carboxylic O atoms distances to the bilayer center. The corresponding distances probability distributions corresponding to the Y4, Y8, and Y12 peptides simulations are depicted in Fig. 8, panels A, B, and C, respectively.

To have a qualitative idea of the comparative reactivity trends between Tyr and LOO• group, we analyzed the overlap between the

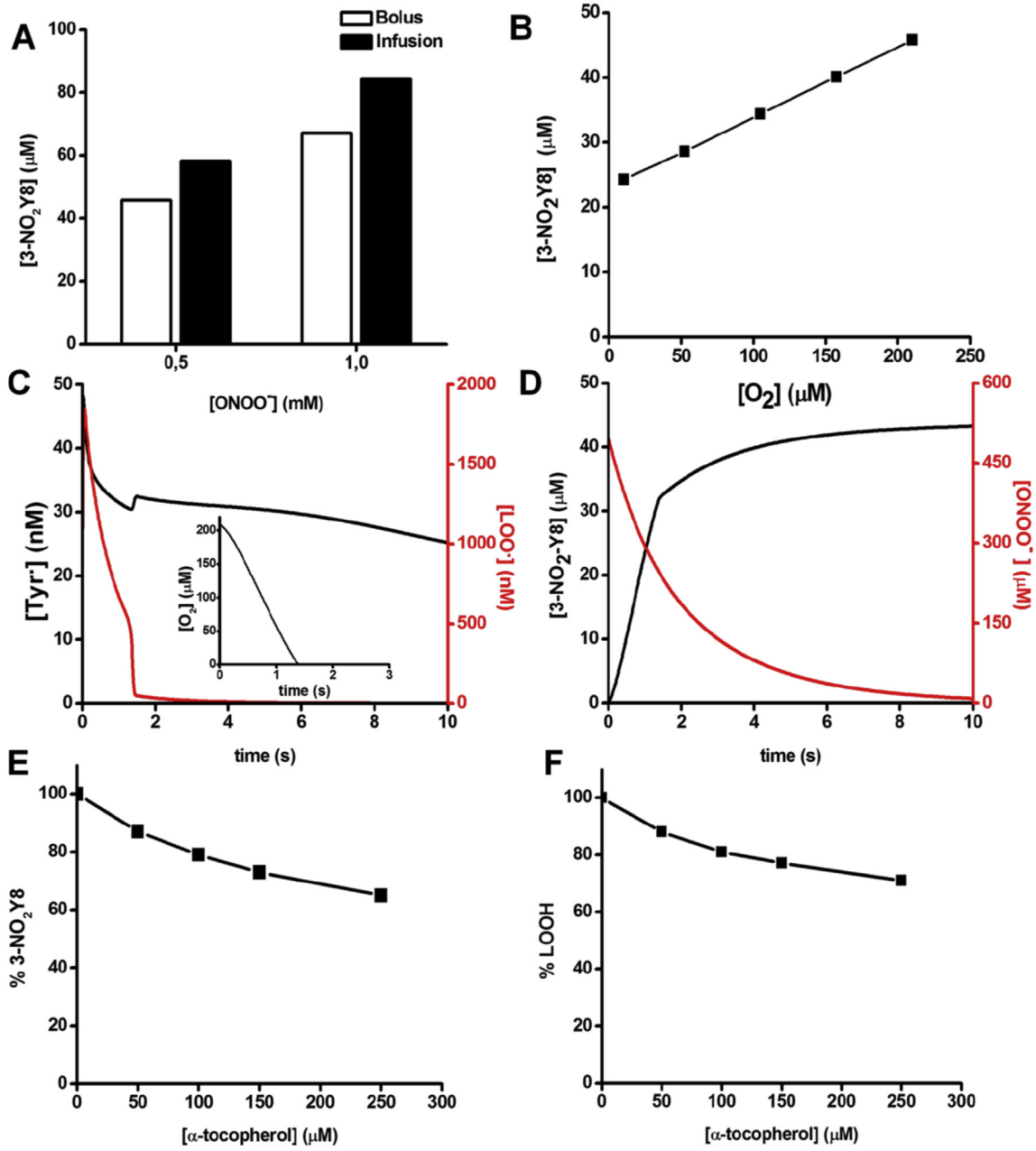

Fig. 6. Kinetic simulations. Computer-assisted simulations considering all equations listed in Table 2 were performed with GEPASI software, using the same experimental tested conditions. The extent of 3-nitrotyrosine yields was evaluated in the presence of peroxynitrite added either as a bolus or slow infusion for the Y8 peptide **(A).** In addition, the influence of molecular oxygen on the extent of 3-nitrotyrosine peptide formation, when peptides were exposed to peroxynitrite added as a single bolus was evaluated; reported oxygen concentrations are those present in solution **(B)**. The time course of the concentration of •Tyr and LOO• radicals and molecular oxygen **(C)**, $ONOO^-$ and 3-NT **(D)** is also shown. Peroxynitrite-dependent peptide nitration **(E)** and lipid hydroperoxides (LOOH) formation **(F)** in the presence and absence of α-tocopherol. The levels of LOOH found in the control system in the simulation were 280 μM, within the same order of magnitude of the experimentally-obtained values. All simulation conditions were the same than those tested experimentally.

phenolic O distance distributions, and those corresponding to C9 and C13. In the Y4 peptide, the z-distribution of the phenolic oxygen significantly overlaps with positions observed for C9, and to a lesser extent to C13. Y4 adopts a dominant conformation that positions the oxygen at about 10 Å from the membrane center. For Y8, as expected, the oxygen is found deeper in the membrane, showing two conformations, the predominant one at about 5 Å and a second one where the oxygen is positioned close to the membrane center ($Z = 0$). In this case, overlap is similar with both C9 and C13 positions of the lipids. Finally, for the Y12 peptide, Tyr adopts a conformation that allows its oxygen to be located close to the membrane center, where it it predominantly -almost exclusively- overlaps with C13.

Another point of notice concerning the reactivity of the tyrosine residues it is related to their solvation. Analysis of our MD simulations, show that water molecules significantly penetrate to the polar heads of the lipids, up to the CO groups. Thus it is clear that while Y12 is completely shielded from water, and Y8 also to a significant extent, Y4 shows significant solvation.

Taking as reference the most reactive Y8 phenolic O distribution overlap with either C9, or C13 distributions, the relative values for Y4, and Y12, are 82 and 51%, respectively.

Table 2
Main reactions involved in tyrosine and peptides containing tyrosine in hydrophobic environments, including lipid peroxidation and its connection with tyrosine nitration and oxidation.

Eq	Reaction	k (M^{-1} s^{-1})	Ref
1	$L + {}^{\bullet}OH \rightarrow L^{\bullet} + OH^{-}$	1×10^{10}	[53]
2	$L + {}^{\bullet}NO_2 \rightarrow L^{\bullet} + NO_2^{-}$	4×10^{4}[a]	[7]
3	$Tyr + {}^{\bullet}OH \rightarrow {}^{\bullet}Tyr + OH^{-}$	1.24×10^{10}	[8]
4	$Tyr + {}^{\bullet}OH \rightarrow {}^{\bullet}TyrOH + OH^{-}$	6.5×10^{8}	[8]
5	$Tyr + {}^{\bullet}NO_2 \rightarrow {}^{\bullet}Tyr + NO_2^{-}$	3.2×10^{5}	[7]
6	$^{\bullet}Tyr + {}^{\bullet}NO_2 \rightarrow$ 3-NO_2-Tyr	3×10^{9}	[7]
7	$^{\bullet}Tyr + {}^{\bullet}Tyr \rightarrow$ di-Tyr	2×10^{2}–2.25×10^{8}	[85]-[this work][b]
8	$L^{\bullet} + O_2 \rightarrow LOO^{\bullet}$	3×10^{8}	[94]
9	$LOO^{\bullet} + L \rightarrow LOOH + L^{\bullet}$	37	[81]
10	$2LOO^{\bullet} \rightarrow LOOH + O_2$	1×10^{7}	[94]
11	$LOO^{\bullet} + L^{\bullet} \rightarrow LOOL$	5×10^{7}	[94]
12	$2\ L^{\bullet} \rightarrow LL$	5×10^{8}	[94]
13	$LOO^{\bullet} + NO_2^{-} \rightarrow LOOH + {}^{\bullet}NO_2$	4.5×10^{6}	[72]
14	$LOO^{\bullet} + Tyr \rightarrow LOOH + {}^{\bullet}Tyr$	4.8×10^{3}	[9]
15	α-tocopherol + $LOO^{\bullet} \rightarrow \alpha$-tocopheryl$^{\bullet}$ + LOOH	1.1×10^{6}	[95]
16	α-tocopheryl$^{\bullet}$ + $LOO^{\bullet} \rightarrow$ 8a-(Lipid-dioxy)-α -tocopherone	1×10^{8}	[73]
17	α-tocopherol + $^{\bullet}NO_2 \rightarrow \alpha$-tocopheryl$^{\bullet}$ + NO_2^{-}	1×10^{5}	[79]
18	α-tocopherol + $^{\bullet}OH \rightarrow \alpha$-tocopheryl$^{\bullet}$ + OH^{-}	3.8×10^{9}	[96]
19	$\rightarrow ONOO^{-}$	0-50 μM/min	
20	$ONOOH \rightarrow {}^{\bullet}NO_2 + {}^{\bullet}OH$	0.11 s^{-1}	[97]
21	$ONOO^{-} \rightarrow NO_3^{-}$	0.26 s^{-1}	[97]
22	$^{\bullet}TyrOH + O_2 \rightarrow$ OH-TyrOO	2×10^{9}	[98]
23	OH-TyrOO $\rightarrow$ TyrOH + $O_2^{\bullet-}$	1.3×10^{5} s^{-1}	[98]
24	$O_2^{\bullet-} + {}^{\bullet}NO \leftrightarrow ONOO^{-}$	$f = 6.7 \times 10^{9}$	[99,100]
		$r = 0.02$ s^{-1}	[101–103]
25	$^{\bullet}NO + {}^{\bullet}NO_2 \leftrightarrow N_2O_3$	$f = 1.1 \times 10^{9}$	[104]
		$r = 8.4 \times 10^{4}$ s^{-1}	
26	$N_2O_3 \rightarrow NO_2^{-} + NO_3^{-} + 2H^{+}$	8×10^{4} s^{-1}	[105,106]
27	$N_2O_3 + ONOO^{-} \rightarrow 2\ {}^{\bullet}NO_2 + NO_2^{-}$	1×10^{7}	[105]
28	$O_2^{\bullet-} + {}^{\bullet}NO_2 \leftrightarrow O_2NOO^{-}$	$f = 4.5 \times 10^{9}$	[100]
		$r = 1.35$ s^{-1}	
29	$2ONOO^{-} \rightarrow O_2NOO^{-} + NO_2^{-}$	2×10^{2}[c]	[107]
30	$^{\bullet}Tyr + {}^{\bullet}NO \leftrightarrow$ TyrONO	$f = 1 \times 10^{9}$	[69,108]
		$r = 1 \times 10^{3}$ s^{-1}	
31	$L + Tyr^{\bullet} \rightarrow L^{\bullet} + Tyr$	1×10^{2}[d]	[9]
32	$\rightarrow O_2$	52 μM/min[e]	

[a] This rate constant value was adjusted from the original reported by Prutz et al. [7] in order to include a reverse reaction leading to the formation of $\bullet NO_2$ through the decomposition of a putative LOO-NO_2 adduct.
[b] With peptides the value of the reaction constant for dimerization was considered as 2×10^{2} M^{-1} s^{-1}, taking into account the decrease in the diffusion coefficient of the peptides compared to free tyrosine.
[c] Apparent rate constant value considering that the peroxynitrite disproportionation reaction involves both the anionic and protonated forms and that ONOOH represents 20% of peroxynitrite at pH 7,4.
[d] The value of this reaction constant was calculated considering the reaction of Tyr as part of a transmembrane peptide.
[e] This value was introduced as a way to replenish the amount of O_2 consumed in the system. For the sake of simplicity, the concentration of oxygen used in the simulations were that of the buffer solution, although is likely that the actual concentration in the liposomes is two to three times higher due to favored partitioning [80]. The most relevant reactions for the reported experimental observations are indicated in bold (Equations (1), (5), (6), (8), (9), (14), (20) and (32)). The "connecting reaction" corresponds to reaction 14.

3. Discussion

Herein, we have explored tyrosine oxidation and nitration in transmembrane tyrosine-containing peptides mediated by biologically-relevant oxidants such as peroxynitrite. The overall tested hypothesis is that in membranes that contain a large excess of phospholipids over other components, the lipid peroxidation process fuels peptide oxidation. Indeed, unsaturated fatty acids (*e.g* linoleic acid) are the preferential target of oxidizing radicals reaching membranes (*e.g.* •OH, $^{\bullet}NO_2$) and therefore peptide/protein oxidation would be related to secondary oxidants formed during the lipid peroxidation process. In particular, we have recently communicated that both lipid LOO• [9] and lipid LO• [10] radicals can readily oxidize tyrosine promoting its one-electron oxidation to tyrosyl radical. In this work, we have used a model system of PC liposomes with pre-incorporated 23-amino acid transmembrane peptides containing a single tyrosine at positions 4, 8 and 12 from the amino terminal. With a phospholipid/peptide ratio of 100 (30 mM/0.3 mM), the hydrophobic tyrosine peptides span through the membrane as an α-helix with Y4, Y8 and Y12 located just below the membrane surface, at half way of a monolayer and at approximately the center of the bilayer, respectively [48] as previously characterized by fluorescence quenching and ESR-spin labeling experiments [50].

The location of the tyrosine in the lipid bilayer is relevant to understand the oxidation processes, as there is more hydrophobicity towards the center of the membrane that can influence key variables in the oxidation process including water distribution partitioning of reactive species (such as $^{\bullet}NO_2$ and O_2) as well as the lateral diffusion of peptide and lipid residues. Moreover, if lipid peroxidation plays a key role in facilitating tyrosine oxidation, the structural relationship between the carbon atoms participating in the fatty acid double bounds (*i.e.* C9 and C13 of linoleic acid where molecular oxygen will add to carbon-centered radicals after H-abstraction by the primary oxidizing radicals at the allylic carbon C11, followed by double bond conjugation) and the tyrosine residue may be relevant. Once, LOO• radicals are formed, these species could promote the oxidation of either an adjacent unsaturated fatty acid (present at high mM concentrations, but with a low rate constant of ~37 $M^{-1}s^{-1}$ [7] [81]) or of tyrosine (present at

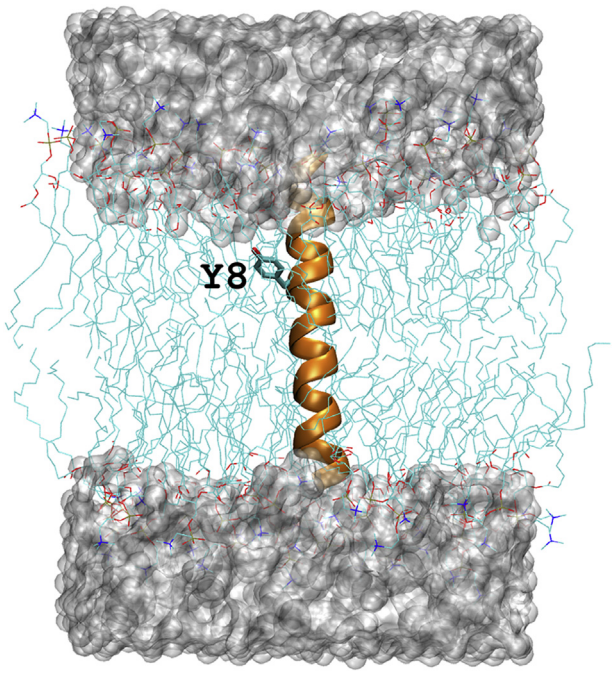

Fig. 7. Schematic representation of a typical snapshot of the Y8 peptide simulation, showing the lipids (light blue thin sticks), water molecules (gray contours), the peptide (yellow ribbon) and the tyrosine residue. (For interpretation of the references to colour in this figure legend, the reader is referred to the web version of this article.)

submilimolar concentration, but with a moderate rate constant of ~4.8 × 10^3 $M^{-1}s^{-1}$ [9]) in a competitive manner (LOO• can be also formed in saturated fatty acids treated with peroxynitrite [9], but are unable to promote lipid oxidation in DPLC). Therefore, at a first glance, an increased level of unsaturation in PC liposomes could result in a decrease of tyrosine oxidation yields. However, peroxynitrite-dependent BTBE nitration and dimerization yields were still high in PC liposomes containing a large polyunsaturated fatty acid content [48].

These data indicate that a simple competition kinetic model does not apply and suggest that lipid-derived radicals mediate tyrosine oxidation within the membrane.

In a seminal report where •NO_2 was generated radiolytically [7], it was found that linoleate in 20-fold excess over a tyrosine-containing dipeptide marginally inhibited •NO_2-mediated tyrosine nitration, in kinetic conditions under which •NO_2 would initially predominantly react with the fatty acid to yield the fatty acid alkyl radical; the lack of significant competition is in agreement with both, lipid-derived radicals promoting the one-electron oxidation of tyrosine, and also a least appreciated phenomena which is the reversible addition of •NO_2 (causing a *cis* to *trans* isomerization of the fatty acid double bonds[2]), that may result in the supply of •NO_2 for the nitration reaction of the tyrosyl radical [7,82,83].

Herein, we were able to recapitulate previous data on BTBE [9,48], as we demonstrated that peroxynitrite-mediated peptide nitration resulted in higher yields for unsaturated liposomes, compared to saturated ones (Fig. 2A–B). In addition, we were able to confirm the participation of lipid radicals on tyrosine nitration, as demonstrated in the experiments where hemin and ABAP were used as oxidants (Fig. 3A–B). Moreover, the presence of bicarbonate inhibited peroxynitrite-mediated peptide nitration (and lipid peroxidation), consistent with the fact that CO_3•$^-$ do not permeate membrane bilayers and that they enhance tyrosine nitration only in hydrophilic milieu, as reported previously [48].

Another interesting observation that supports the connection between lipid and tyrosine oxidation relates to the comparative tyrosine nitration yields of bolus *vs* infusion of peroxynitrite. It is well established and reported that nitration yields for free tyrosine or hydrophilic analogs such as pHPA are lower when peroxynitrite is slowly infused mainly because of the preferential consumption of •NO_2 by direct reaction with tyrosine instead of the recombination reaction with tyrosyl radicals (these latter formed at high yields during bolus addition). In sharp contrast, nitration yields in both BTBE and the hydrophobic tyrosine peptides were significantly larger during infusion in comparison to bolus (Fig. 2). This notable phenomenon may be due to a series of factors but indicates a clear difference of underlying mechanisms of tyrosine nitration in hydrophilic *vs* hydrophobic phases; the main reasons of this disparate

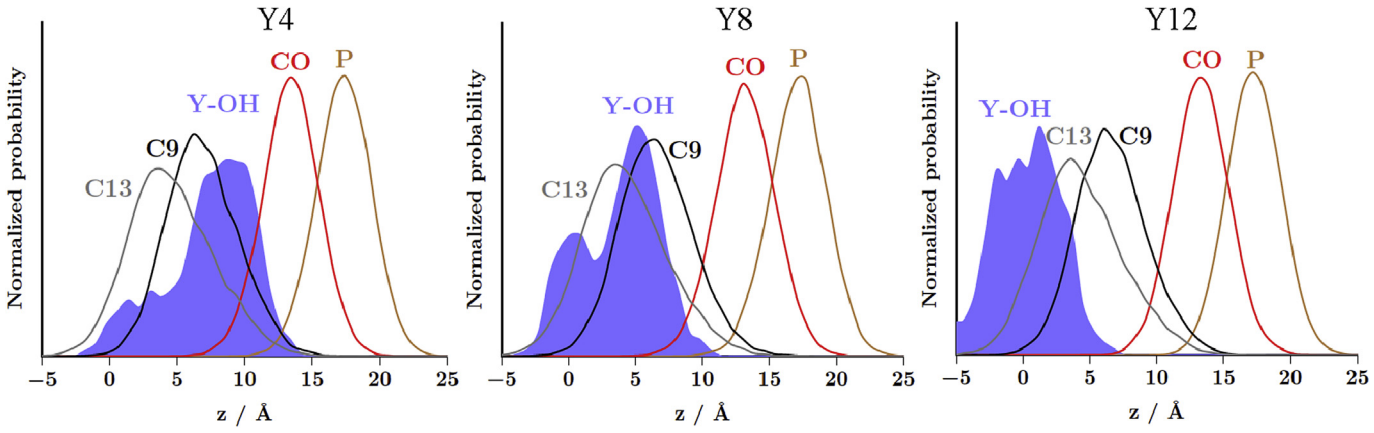

Fig. 8. Probability of localization of the different atoms in the length of the bilayer. Comparison of relevant functional groups (either phosphate, carbonyl, C9, C13, and phenolic O) localization distribution along the bilayer normal, extracted from the MD simulations. The z positions are given relative to the bilayer center (z = 0). The purple distribution corresponds to the phenolic O atom. The different atoms are represented with different colours. Phosphorous (brown), carbonylic oxygen (red), lipid C9 (dark grey), C13 (light grey) and tyrosine (purple). (For interpretation of the references to colour in this figure legend, the reader is referred to the web version of this article.)

[2] A few percent of the added •NO_2 yields nitrated fatty acid derivatives [82].

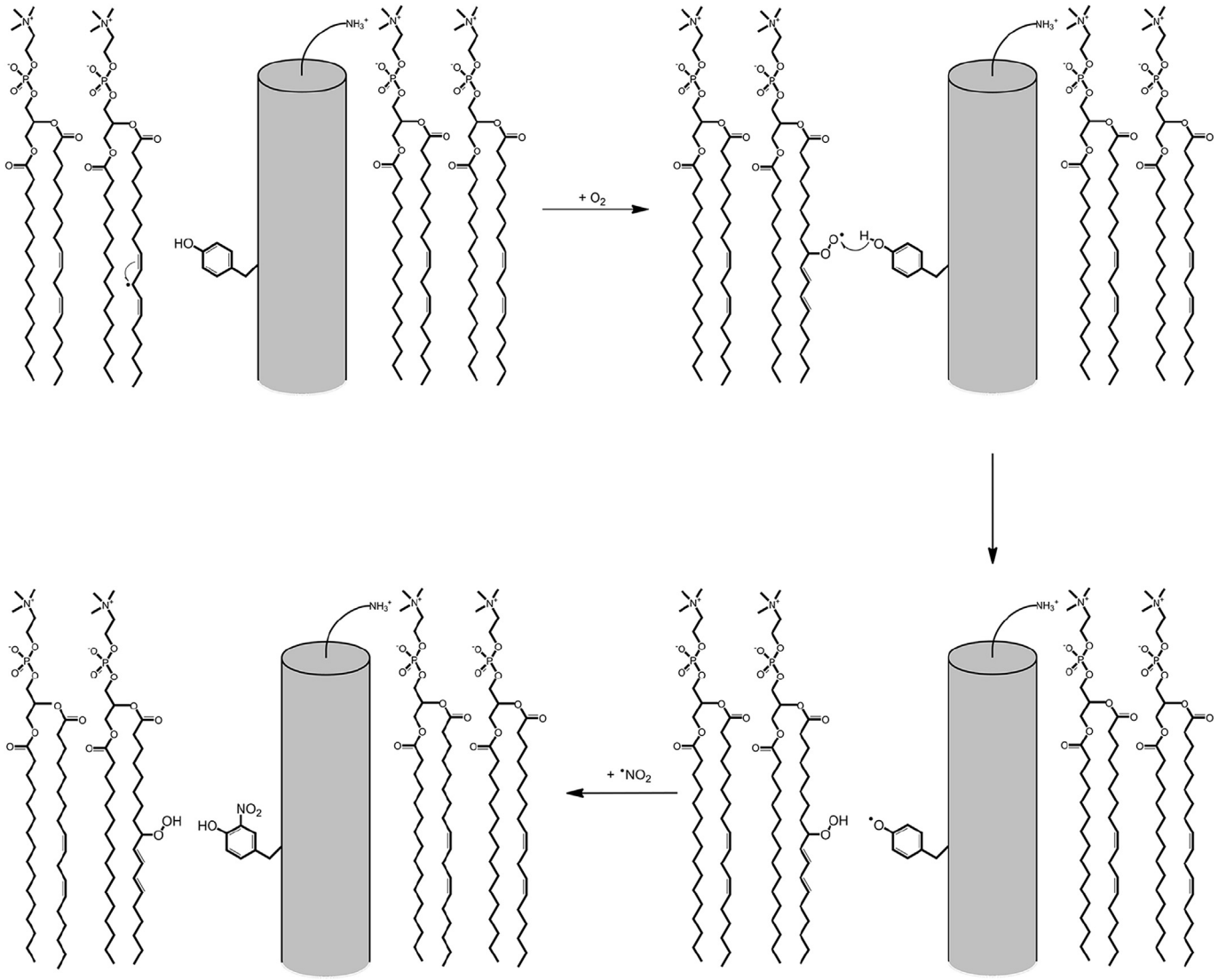

Fig. 9. Proposed reaction mechanism that connects lipid peroxidation and peptide oxidation and nitration in membranes. The initial step involves the one-electron oxidation of the allylic hydrogen by peroxynitrite-derived radicals ($^{\bullet}OH$ and $^{\bullet}NO_2$) or ABAP-derived peroxyl radicals, yielding the lipid-derived alkyl radical (structure shown in the upper left). The following steps are indicated and result in the nitration of the tyrosine-containing transmembrane peptide (lower left).

result are that a) in membranes the process of tyrosyl radical dimerization is marginal (Eq. (7)) due to the much slower diffusion of the transmembrane tyrosine peptide (estimated D ~ 1000 *vs* 0.5 $\mu m^2 s^{-1}$ for free tyrosine in solution and membrane-associated peptide [9,48], together with b) a reversible reaction of $^{\bullet}NO_2$ with unsaturated lipids providing a flux of the proximal species for tyrosine nitration (see also Eq. (2), Table 2).

The effects of molecular oxygen levels in tyrosine nitration yields were remarkable for both the tyrosine-containing peptides as well as for BTBE. However, the peroxynitrite-dependent nitration of free tyrosine was insensitive to oxygen levels in the 1–21% range (*ca.* 10–210 μM in solution), in agreement with the reportedly low or no reactivity of tyrosyl radical with molecular oxygen ($<10^3$ $M^{-1}s^{-1}$, [84,85]; indeed, molecular oxygen does not affect tyrosine dimerization yields from recombination of tyrosyl radicals either [9,84].[3] Thus, the effects of oxygen in promoting the nitration of the hydrophobic tyrosine analogs Y8 and BTBE are due to its participation in the lipid peroxidation process through its diffusion-controlled reaction with alkyl radicals to yield the corresponding peroxyl radical. The selectivity of the molecular oxygen reaction in our liposomal system represents strong evidence of the connection of the lipid peroxidation with the tyrosine oxidation process in hydrophobic biostructures (Fig. 4A–F). The effect of molecular oxygen on peptide nitration yields was nicely recapitulated in computer-assisted simulations with an overall trend that was independent of the actual solution/membrane partition ratio of O_2 ranging from one (Fig. 6) to three (Fig. S2, Supporting Information).

The observed inhibitory effect of α-tocopherol is in agreement with its expected reaction with lipid peroxyl radicals ($k = 1 \times 10^8$ $M^{-1}s^{-1}$ [73]) (Fig. 5) and was recapitulated by kinetic simulations (Fig. 6) considering an overall stoichiometry factor of two (Eqs. (15) and (16), Table 2). Once formed, the lipid peroxyl radical, which is a polar center, usually diffuses out from the apolar

[3] The lack or minimal reactivity of tyrosyl radical with molecular oxygen [84] is not shared by other amino acid-derived radicals which evolve to peroxyl radicals.

interior of the lipid bilayer to surface towards the microenvironment where the redox active phenolic moiety of tocopherol [86,87]. In cases where diffusion towards the lipid-water interphase of the LOO• may be limited [88], the chromanol group in α-tocopherol may exert its actions by penetrating to some extent into the bilayer [87]. It is important to note that irrespective of participating rate constant values during the inhibitory action of α-tocopherol on peptide nitration, the lateral diffusion coefficient in membranes of α-tocopherol is about one order of magnitude higher (*ca.* 10 $\mu m^2 s^{-1}$ [89]), than that of phosphatidylcholine *ca.* 1 $\mu m^2 s^{-1}$ and the transmembrane peptides *ca.* 0.5 $\mu m^2 s^{-1}$ [9,90] thus, the mutual lateral diffusion coefficient[4] of the LOO• with α-tocopherol is about 10-times higher than that of LOO• with the transmembrane peptides.

Finally, computational studies (Fig. 8) analyzed the relevance of the overlay of the tyrosine moeities of Y4, Y8 and Y12 with the LOO• formed in either C-9 or C-13 of linoleic acid to account for the differential yields of tyrosine nitration in the three peptides (Fig. 2). In the case of Y8, its largest overlay was in agreement with the largest nitration yield. In Y12, however, another key factor such as the favored partioning of $•NO_2$ in the hydrophobic core of the membrane [9] is likely to explain its relative favorable nitration yield in comparison to Y4.

In summary, in this manuscript we have confirmed that in membranes tyrosine oxidation and nitration is connected to the lipid peroxidation process (Fig. 9). Due to the ubiquity of unsaturated fatty acids in biomembranes (and lipoproteins) primary radical species will preferentially react firstly with them to initiate the oxidation process in the hydrophobic biostructure. Then, lipid peroxidation is an oxygen-dependent process that results in the formation of peroxyl (LOO•) (Eq. (8)) and, secondarily, alkoxyl radicals (LO•) [91–93]. These lipid-derived radicals are reactive species that can in turn oxidize biological targets (RH) including protein side chains. Our work confirmed that tyrosine residues located at different depths of the model membrane were oxidized by lipid-derived radicals, that the process is critically influenced by oxygen levels and can be modulated by tocopherols. The paper also addresses how structural relationships between lipids and transmembrane peptides could influence the oxidation process, where reactivity and diffusion become competing processes. The data with tocopherols, that exert most of its chain breaking action near the lipid-water interphase, indicate that the diffusion of LOO• from the interior of the bilayer to the membrane surface is fast enough to outcompete the relatively slow reactions of LOO• with either LH or tyrosine residues. The experimental data provided herein with the use of transmembrane peptides together with computational-assisted kinetic and molecular dynamic analysis allows to rationalize protein oxidation and nitration processes fueled by lipid peroxidation reactions in hydrophobic bio-structures.

Acknowledgments

This work was supported by grants of Agencia Nacional de Investigación e Innovación (Fondo Clemente Estable, FCE_6605) to S.B. and Universidad de la República (CSIC and EI) and National Institutes of Health (RO1 AI095173) to R.R. Additional funding to S.B. and R.R. was provided by Aldenor, Ridaline and ASM through Fundación Manuel Pérez, Facultad de Medicina, Universidad de la República, Uruguay. D.M.M was supported by postdoctoral fellowships from CNPq (203400/2014-3) and International Centre of Genetic Engineering and Biotechnology (ICGEB, Trieste).

[4] The mutual lateral diffusion coefficient is the sum of the individual diffusion coefficients [89].

Appendix A. Supplementary data

Supplementary data related to this article can be found at http://dx.doi.org/10.1016/j.abb.2017.04.006.

References

[1] R. Radi, Nitric oxide, oxidants, and protein tyrosine nitration, Proc. Natl. Acad. Sci. U. S. A. 101 (2004) 4003–4008.
[2] R. Radi, Protein tyrosine nitration: biochemical mechanisms and structural basis of its functional effects, Accounts Chem. Res. 46 (2013) 550–559.
[3] R. Radi, Peroxynitrite, a stealthy biological oxidant, J. Biol. Chem. 288 (2013) 26464–26472.
[4] C. Batthyany, S. Bartesaghi, M. Mastrogiovanni, A. Lima, V. Demicheli, R. Radi, Tyrosine-nitrated proteins: proteomic and bioanalytical aspects, Antioxid. Redox Signal 26 (2017) 313–328.
[5] N. Campolo, S. Bartesaghi, R. Radi, Metal-catalyzed protein tyrosine nitration in biological systems, Redox Rep. 19 (2014) 221–231.
[6] A. Denicola, B.A. Freeman, M. Trujillo, R. Radi, Peroxynitrite reaction with carbon dioxide/bicarbonate: kinetics and influence on peroxynitrite-mediated oxidations, Arch. Biochem. Biophys. 333 (1996) 49–58.
[7] W.A. Prutz, H. Monig, J. Butler, E.J. Land, Reactions of nitrogen dioxide in aqueous model systems: oxidation of tyrosine units in peptides and proteins, Arch. Biochem. Biophys. 243 (1985) 125–134.
[8] S. Solar, W. Solar, N. Getoff, Reactivity of OH with tyrosine in aqueous solution studie by pulse radiolysis, J. Phys. Chem. 88 (1984) 2091–2095.
[9] S. Bartesaghi, J. Wenzel, M. Trujillo, M. Lopez, J. Joseph, B. Kalyanaraman, R. Radi, Lipid peroxyl radicals mediate tyrosine dimerization and nitration in membranes, Chem. Res. Toxicol. 23 (2010) 821–835.
[10] L.K. Folkes, S. Bartesaghi, M. Trujillo, R. Radi, P. Wardman, Kinetics of oxidation of tyrosine by a model alkoxyl radical, Free Radic. Res. 46 (2012) 1150–1156.
[11] G. Ferrer-Sueta, D. Vitturi, I. Batinic-Haberle, I. Fridovich, S. Goldstein, G. Czapski, R. Radi, Reactions of manganese porphyrins with peroxynitrite and carbonate radical anion, J. Biol. Chem. 278 (2003) 27432–27438.
[12] L.A. Marquez, H.B. Dunford, Kinetics of oxidation of tyrosine and dityrosine by myeloperoxidase compounds I and II. Implications for lipoprotein peroxidation studies, J. Biol. Chem. 270 (1995) 30434–30440.
[13] J.M. Souza, G. Peluffo, R. Radi, Protein tyrosine nitration–functional alteration or just a biomarker? Free Radic. Biol. Med. 45 (2008) 357–366.
[14] L. Thomson, 3-nitrotyrosine modified proteins in atherosclerosis, Dis. Markers. 2015 (2015) 708282.
[15] I. Parastatidis, L. Thomson, D.M. Fries, R.E. Moore, J. Tohyama, X. Fu, S.L. Hazen, H.F. Heijnen, M.K. Dennehy, D.C. Liebler, Increased protein nitration burden in the atherosclerotic lesions and plasma of apolipoprotein AI–deficient mice, Circulation Res. 101 (2007) 368–376.
[16] Y. Huang, J.A. DiDonato, B.S. Levison, D. Schmitt, L. Li, Y. Wu, J. Buffa, T. Kim, G.S. Gerstenecker, X. Gu, An abundant dysfunctional apolipoprotein A1 in human atheroma, Nat. Med. 20 (2014) 193–203.
[17] J.A. DiDonato, K. Aulak, Y. Huang, M. Wagner, G. Gerstenecker, C. Topbas, V. Gogonea, A.J. DiDonato, W.H. Tang, R.A. Mehl, P.L. Fox, E.F. Plow, J.D. Smith, E.A. Fisher, S.L. Hazen, Site-specific nitration of apolipoprotein AI at tyrosine 166 is both abundant within human atherosclerotic plaque and dysfunctional, J. Biol. Chem. 289 (2014) 10276–10292.
[18] D.A. Capdevila, S. Oviedo Rouco, F. Tomasina, V. Tortora, V. Demicheli, R. Radi, D.H. Murgida, Active site structure and peroxidase activity of oxidatively modified cytochrome c species in complexes with cardiolipin, Biochemistry 54 (2015) 7491–7504.
[19] J.P. L.A.C. MacMillan-Crow, J.D. Kerby, J.S. Beckman, J.A. Thompson, Nitration and inactivation of manganese superoxide dismutase in chronic rejection of human renal allgrafts, Proc Natl Acad Sci U. S. A. 93 (1996) 11853–11858.
[20] C. Szabo, H. Ischiropoulos, R. Radi, Peroxynitrite: biochemistry, pathophysiology and development of therapeutics, Nat. Rev. Drug Discov. 6 (2007) 662–680.
[21] J.S. Beckman, H. Ischiropoulos, L. Zhu, M. van der Woerd, C. Smith, J. Chen, J. Harrison, J.C. Martin, M. Tsai, Kinetics of superoxide dismutase- and iron-catalyzed nitration of phenolics by peroxynitrite, Arch. Biochem. Biophys. 298 (1992) 438–445.
[22] A.M. Cassina, R. Hodara, J.M. Souza, L. Thomson, L. Castro, H. Ischiropoulos, B.A. Freeman, R. Radi, Cytochrome c nitration by peroxynitrite, J. Biol. Chem. 275 (2000) 21409–21415.
[23] S.K. Kong, M.B. Yim, E.R. Stadtman, P.B. Chock, Peroxynitrite disables the tyrosine phosphorylation regulatory mechanism: lymphocyte-specific tyrosine kinase fails to phosphorylate nitrated cdc2(6-20)NH2 peptide, Proc. Natl. Acad. Sci. U. S. A. 93 (1996) 3377–3382.
[24] M. Tien, B.S. Berlett, R.L. Levine, P.B. Chock, E.R. Stadtman, Peroxynitrite-mediated modification of proteins at physiological carbon dioxide concentration: pH dependence of carbonyl formation, tyrosine nitration, and methionine oxidation, Proc. Natl. Acad. Sci. U. S. A. 96 (1999) 7809–7814.
[25] J.S. Beckman, Y.Z. Ye, P.G. Anderson, J. Chen, M.A. Accavitti, M.M. Tarpey, C.R. White, Extensive nitration of protein tyrosines in human atherosclerosis detected by immunohistochemistry, Biol. Chem. Hoppe Seyler 375 (1994) 81–88.

[26] L.W. Velsor, C.A. Ballinger, J. Patel, E.M. Postlethwait, Influence of epithelial lining fluid lipids on NO2-induced membrane oxidation and nitration, Free Radic. Biol. Med. 34 (2003) 720–733.
[27] M.A. Adgent, G.L. Squadrito, C.A. Ballinger, D.M. Krzywanski, J.R. Lancaster, E.M. Postlethwait, Desferrioxamine inhibits protein tyrosine nitration: mechanisms and implications, Free Radic. Biol. Med. 53 (2012) 951–961.
[28] N. Romero, G. Peluffo, S. Bartesaghi, H. Zhang, J. Joseph, B. Kalyanaraman, R. Radi, Incorporation of the hydrophobic probe N-t-BOC-L-tyrosine tert-butyl ester to red blood cell membranes to study peroxynitrite-dependent reactions, Chem. Res. Toxicol. 20 (2007) 1638–1648.
[29] B. Shao, C. Bergt, X. Fu, P. Green, J.C. Voss, M.N. Oda, J.F. Oram, J.W. Heinecke, Tyrosine 192 in apolipoprotein A-I is the major site of nitration and chlorination by myeloperoxidase, but only chlorination markedly impairs ABCA1-dependent cholesterol transport, J. Biol. Chem. 280 (2005) 5983–5993.
[30] S.L. Hazen, R. Zhang, Z. Shen, W. Wu, E.A. Podrez, J.C. MacPherson, D. Schmitt, S.N. Mitra, C. Mukhopadhyay, Y. Chen, P.A. Cohen, H.F. Hoff, H.M. Abu-Soud, Formation of nitric oxide-derived oxidants by myeloperoxidase in monocytes: pathways for monocyte-mediated protein nitration and lipid peroxidation in vivo, Circ. Res. 85 (1999) 950–958.
[31] R. Zhang, M.L. Brennan, X. Fu, R.J. Aviles, G.L. Pearce, M.S. Penn, E.J. Topol, D.L. Sprecher, S.L. Hazen, Association between myeloperoxidase levels and risk of coronary artery disease, Jama 286 (2001) 2136–2142.
[32] L. Zheng, B. Nukuna, M.L. Brennan, M. Sun, M. Goormastic, M. Settle, D. Schmitt, X. Fu, L. Thomson, P.L. Fox, H. Ischiropoulos, J.D. Smith, M. Kinter, S.L. Hazen, Apolipoprotein A-I is a selective target for myeloperoxidase-catalyzed oxidation and functional impairment in subjects with cardiovascular disease, J. Clin. Invest 114 (2004) 529–541.
[33] L. Zheng, M. Settle, G. Brubaker, D. Schmitt, S.L. Hazen, J.D. Smith, M. Kinter, Localization of nitration and chlorination sites on apolipoprotein A-I catalyzed by myeloperoxidase in human atheroma and associated oxidative impairment in ABCA1-dependent cholesterol efflux from macrophages, J. Biol. Chem. 280 (2005) 38–47.
[34] T.K. Hsiai, J. Hwang, M.L. Barr, A. Correa, R. Hamilton, M. Alavi, M. Rouhanizadeh, E. Cadenas, S.L. Hazen, Hemodynamics influences vascular peroxynitrite formation: implication for low-density lipoprotein apo-B-100 nitration, Free Radic. Biol. Med. 42 (2007) 519–529.
[35] C. Mallozzi, A.M. Di Stasi, M. Minetti, Peroxynitrite modulates tyrosine-dependent signal transduction pathway of human erythrocyte band 3, Faseb J. 11 (1997) 1281–1290.
[36] G. Celedón, G. González, J. Pino, E.A. Lissi, Peroxynitrite oxidizes erythrocyte membrane band 3 protein and diminishes its anion transport capacity, Free Radic. Res. 41 (2007) 316–323.
[37] J. Murray, S.W. Taylor, B. Zhang, S.S. Ghosh, R.A. Capaldi, Oxidative damage to mitochondrial complex I due to peroxynitrite: identification of reactive tyrosines by mass spectrometry, J. Biol. Chem. 278 (2003) 37223–37230.
[38] S.J. Chinta, J.K. Andersen, Nitrosylation and nitration of mitochondrial complex I in Parkinson's disease, Free Radic. Res. 45 (2011) 53–58.
[39] R.I. Viner, D.A. Ferrington, T.D. Williams, D.J. Bigelow, C. Schoneich, Protein modification during biological aging: selective tyrosine nitration of the SERCA2a isoform of the sarcoplasmic reticulum Ca2+-ATPase in skeletal muscle, Biochem. J. 340 (1999) 657–669.
[40] S. Xu, J. Ying, B. Jiang, W. Guo, T. Adachi, V. Sharov, H. Lazar, J. Menzoian, T.V. Knyushko, D.J. Bigelow, C. Schoneich, R.A. Cohen, Detection of sequence-specific tyrosine nitration of manganese SOD and SERCA in cardiovascular disease and aging, AJP-Heart 290 (2006) 2220–2227.
[41] T.V. Knyushko, V.S. Sharov, T.D. Williams, C. Schöneich, D.J. Bigelow, 3-Nitrotyrosine modification of SERCA2a in the aging heart: a distinct signature of the cellular redox environment, Biochemistry 44 (2005) 13071–13081.
[42] M.K. Strosova, J. Karlovska, P. Zizkova, M. Kwolek-Mirek, S. Ponist, C.M. Spickett, L. Horakova, Modulation of sarcoplasmic/endoplasmic reticulum Ca 2+-ATPase activity and oxidative modification during the development of adjuvant arthritis, Archives Biochem. Biophy. 511 (2011) 40–47.
[43] Y. Ji, I. Neverova, J.E. Van Eyk, B.M. Bennet, Nitration of tyrosine 92 mediates the activation of rat microsomal glutathione-S-transferase by peroxynitrite, J. Biol. Chem. 281 (2006) 1986–1991.
[44] T.E. Creighton (Ed.), Proteins: Structures and Molecular Properties, second ed., W.H. Freeman, Oxford, 1992.
[45] S. Bartesaghi, G. Ferrer-Sueta, G. Peluffo, V. Valez, H. Zhang, B. Kalyanaraman, R. Radi, Protein tyrosine nitration in hydrophilic and hydrophobic environments, Amino Acids 32 (2007) 501–515.
[46] B. Shao, S. Pennathur, J.W. Heinecke, Myeloperoxidase targets apolipoprotein A-I, the major high density lipoprotein protein, for site-specific oxidation in human atherosclerotic lesions, J Biol Chem. 287 (2012) 6375–6386.
[47] S. Carballal, S. Bartesaghi, R. Radi, Kinetic and mechanistic considerations to assess the biological fate of peroxynitrite, Biochimica Biophysica Acta (BBA)-General Subj. 1840 (2014) 768–780.
[48] S. Bartesaghi, V. Valez, M. Trujillo, G. Peluffo, N. Romero, H. Zhang, B. Kalyanaraman, R. Radi, Mechanistic studies of peroxynitrite-mediated tyrosine nitration in membranes using the hydrophobic probe *N-t*-BOC-L-tyrosine *tert*-Butyl Ester, Biochemistry 45 (2006) 6813–6825.
[49] H. Zhang, J. Joseph, J. Feix, N. Hogg, B. Kalyanaraman, Nitration and oxidation of a hydrophobic tyrosine probe by peroxynitrite in membranes: comparison with nitration and oxidation of tyrosine by peroxynitrite in aqueous solution, Biochemistry 40 (2001) 7675–7686.
[50] H. Zhang, K. Bhargava, A. Keszler, J. Feix, N. Hogg, J. Joseph, B. Kalyanaraman, Transmembrane nitration of hydrophobic tyrosyl peptides. Localization, characterization, mechanism of nitration, and biological implications, J. Biol. Chem. 278 (2003) 8969–8978.
[51] A. Holt, J.A. Killian, Orientation and dynamics of transmembrane peptides: the power of simple models, Eur. Biophys. J. 39 (2010) 609–621.
[52] D.M. Pahlke, U. Diederichsen, Synthesis and characterization of β-peptide helices as transmembrane domains in lipid model membranes, J. Pept. Sci. 22 (2016) 636–641.
[53] G.V. Buxton, G.L. Greenstock, W.P. Helman, A.B. Ross, J. Phys. Chem. Ref. Data 17 (1988) 513–886.
[54] R. Radi, J.S. Beckman, K.M. Bush, B.A. Freeman, Peroxynitrite oxidation of sulfhydryls. The cytotoxic potential of superoxide and nitric oxide, J. Biol. Chem. 266 (1991) 4244–4250.
[55] R. Radi, J.S. Beckman, K.M. Bush, B.A. Freeman, Peroxynitrite-induced membrane lipid peroxidation: the cytotoxic potential of superoxide and nitric oxide, Arch. Biochem. Biophys. 288 (1991) 481–487.
[56] V.E. Kagan, R.A. Bakalova, Z.Z. Zhelev, D.S. Rangelova, E.A. Serbinova, V.A. Tyurin, N.K. Denisova, L. Packer, Intermembrane transfer and antioxidant action of alpha-tocopherol in liposomes, Arch. Biochem. Biophys. 280 (1990) 147–152.
[57] W.H. Koppenol, J.J. Moreno, W.A. Pryor, H. Ischiropoulos, J.S. Beckman, Peroxynitrite, a cloaked oxidant formed by nitric oxide and superoxide, Chem. Res. Toxicol. 5 (1992) 834–842.
[58] Z.Y. Jiang, A.C. Woollard, S.P. Wolff, Lipid hydroperoxide measurement by oxidation of Fe2+ in the presence of xylenol orange. Comparison with the TBA assay and an iodometric method, Lipids 26 (1991) 853–856.
[59] H. Yin, N.A. Porter, Specificity of the ferrous oxidation of xylenol orange assay: analysis of autoxidation products of cholesteryl arachidonate, Anal. Biochem. 313 (2003) 319–326.
[60] P. Mendes, Biochemistry by numbers: simulation of biochemical pathways with Gepasi 3, Trends Biochem. Sci. 22 (1997) 361–363.
[61] P. Mendes, D. Kell, Non-linear optimization of biochemical pathways: applications to metabolic engineering and parameter estimation, Bioinformatics 14 (1998) 869–883.
[62] V. Demicheli, D.M. Moreno, G.E. Jara, A. Lima, S. Carballal, N. Rios, C. Batthyany, G. Ferrer-Sueta, C. Quijano, D.A. Estrin, M.A. Marti, R. Radi, Mechanism of the reaction of human manganese superoxide dismutase with peroxynitrite: nitration of critical tyrosine 34, Biochemistry 55 (2016) 3403–3417.
[63] V. Demicheli, C. Quijano, B. Alvarez, R. Radi, Inactivation and nitration of human superoxide dismutase (SOD) by fluxes of nitric oxide and superoxide, Free Radic. Biol. Med. 42 (2007) 1359–1368.
[64] J.B. Klauda, R.M. Venable, J.A. Freites, J.W. O'Connor, D.J. Tobias, C. Mondragon-Ramirez, I. Vorobyov, A.D. MacKerell Jr., R.W. Pastor, Update of the CHARMM all-atom additive force field for lipids: validation on six lipid types, J. Phys. Chem. B 114 (2010) 7830–7843.
[65] J.C. Phillips, R. Braun, W. Wang, J. Gumbart, E. Tajkhorshid, E. Villa, C. Chipot, R.D. Skeel, L. Kale, K. Schulten, Scalable molecular dynamics with NAMD, J. Comput. Chem. 26 (2005) 1781–1802.
[66] M. Harvey, G. De Fabritiis, An implementation of the smooth particle mesh Ewald method on GPU hardware, J. Chem. Theory Comput. 5 (2009) 2371–2377.
[67] T. Darden, D. York, L. Pedersen, Particle meshEwald: an N log(N) method for Ewald sums in large systems, J Chem Phys 98 (1993) 10089.
[68] R.R.C. New (Ed.), Liposomes a Practical Approach, Oxford University Press, 1990.
[69] S. Goldstein, G. Czapski, J. Lind, G. Merenyi, Tyrosine nitration by simultaneous generation of (.)NO and O-(2) under physiological conditions. How the radicals do the job, J. Biol. Chem. 275 (2000) 3031–3036.
[70] S. Pfeiffer, K. Schmidt, B. Mayer, Dityrosine formation outcompetes tyrosine nitration at low steady-state concentrations of peroxynitrite implications for tyrosine modification by nitric oxide/superoxide in vivo, J. Biol. Chem. 275 (2000) 6346–6352.
[71] B. Kalyanaraman, C. Mottley, R.P. Mason, A direct electron spin resonance and spin-trapping investigation of peroxyl free radical formation by hematin/hydroperoxide systems, J. Biol. Chem. 258 (1983) 3855–3858.
[72] A. El-Agamey, Laser flash photolysis of new water-soluble peroxyl radical precursor, J Photochem Photobiolo A Chem 203 (2009) 13–17.
[73] D.C. Liebler, J.A. Burr, Oxidation of vitamin E during iron-catalyzed lipid peroxidation: evidence for electron-transfer reactions of the tocopheroxyl radical, Biochemistry 31 (1992) 8278–8284.
[74] R.J. Singh, S.P. Goss, J. Joseph, B. Kalyanaraman, Nitration of gamma-tocopherol and oxidation of alpha-tocopherol by copper-zinc superoxide dismutase/H2O2/NO2-: role of nitrogen dioxide free radical, Proc. Natl. Acad. Sci. U. S. A. 95 (1998) 12912–12917.
[75] O. Augusto, R.M. Gatti, R. Radi, Spin-trapping studies of peroxynitrite decomposition and of 3- morpholinosydnonimine N-ethylcarbamide autooxidation: direct evidence for metal-independent formation of free radical intermediates, Arch. Biochem. Biophys. 310 (1994) 118–125.
[76] O.V. Gerasimov, S.V. Lymar, The yield of hydroxyl radical from the decomposition of peroxynitrous acid, Inorg. Chem. 38 (1999) 4317–4321.
[77] S. Goldstein, S.V. Lymar, Direct and indirect oxidations by peroxynitrite, Inorg. Chem. 34 (1995) 4041–4048.
[78] D.J.W. Barber, J.K. Thomas, Reactions of radicals with lecithin bilayers, Radiat.

Res. 74 (1978) 51–65.
[79] M.J. Davies, L.G. Forni, R.L. Willson, Vitamin E analogue Trolox C. E.s.r. and pulse-radiolysis studies of free-radical reactions, Biochem. J. 255 (1988) 513–522.
[80] M.N. Moller, Q. Li, M. Chinnaraj, H.C. Cheung, J.R. Lancaster Jr., A. Denicola, Solubility and diffusion of oxygen in phospholipid membranes, Biochim. Biophys. Acta 1858 (2016) 2923–2930.
[81] J.M. Gebicki, B.H.J. Bielski, Comparison of the capacities of the perhydroxyl and the superoxide radicals to initiate chain oxidation of linoleic acid, J. Am. Chem. Soc. 103 (1981) 7020–7022.
[82] H. Jiang, N. Kruger, D.R. Lahiri, D. Wang, J.M. Vatele, M. Balazy, Nitrogen dioxide induces cis-trans-isomerization of arachidonic acid within cellular phospholipids. Detection of trans-arachidonic acids in vivo, J. Biol. Chem. 274 (1999) 16235–16241.
[83] C. Ferreri, A. Samadi, F. Sassatelli, L. Landi, C. Chatgilialoglu, Regioselective cis-trans isomerization of arachidonic double bonds by thiyl radicals: the influence of phospholipid supramolecular organization, J. Am. Chem. Soc. 126 (2004) 1063–1072.
[84] E.P. Hunter, M.F. Desrosiers, M.G. Simic, The effect of oxygen, antioxidants, and superoxide radical on tyrosine phenoxyl radical dimerization, Free Radic. Biol. Med. 6 (1989) 581–585.
[85] F. Jin, J. Leicht, C. von Sonntag, The superoxide radical reacts with tyrosine-derived phenoxyl radicals by addition rather than by electron transfer, J. Chem. Soc. Perkin Trans. 2 (1993) 1583–1588.
[86] S.C. Mojumdar, D.A. Becker, G.A. DiLabio, J.J. Ley, L.R. Barclay, K.U. Ingold, Kinetic studies on stilbazulenyl-bis-nitrone (STAZN), a nonphenolic chain-breaking antioxidant in solution, micelles, and lipid membranes, J. Org. Chem. 69 (2004) 2929–2936.
[87] X. Leng, J.J. Kinnun, D. Marquardt, M. Ghefli, N. Kucerka, J. Katsaras, J. Atkinson, T.A. Harroun, S.E. Feller, S.R. Wassall, Alpha-tocopherol is well designed to protect polyunsaturated phospholipids: MD simulations, Biophys. J. 109 (2015) 1608–1618.
[88] J. Garrec, A. Monari, X. Assfeld, L.M. Mir, M. Tarek, Lipid peroxidation in membranes: the peroxyl radical does not “float”, J. Phys. Chem. Lett. 5 (2014) 1653–1658.
[89] G. Gramlich, J. Zhang, W.M. Nau, Diffusion of alpha-tocopherol in membrane models: probing the kinetics of vitamin E antioxidant action by fluorescence in real time, J. Am. Chem. Soc. 126 (2004) 5482–5492.
[90] E. Sackmann, H. Trauble, H. Galla, P. Overath, Lateral diffusion, protein mobility and phase transitions in Escherichia coli membranes. A spin label study, Biochemistry 12 (1973) 5360–5369.
[91] S.H. Lee, T. Oe, I.A. Blair, Vitamin C-induced decomposition of lipid hydroperoxides to endogenous genotoxins, Science 292 (2001) 2083–2086.
[92] E. Niki, Y. Yoshida, Y. Saito, N. Noguchi, Lipid peroxidation: mechanisms, inhibition, and biological effects, Biochem. Biophys. Res. Commun. 338 (2005) 668–676.
[93] A.L. Wilcox, L.J. Marnett, Polyunsaturated fatty acid alkoxyl radicals exist as carbon-centered epoxyallylic radicals: a key step in hydroperoxide-amplified lipid peroxidation, Chem. Res. Toxicol. 6 (1993) 413–416.
[94] C.F. Babbs, M.G. Steiner, Simulation of free radical reactions in biology and medicine: a new two-compartment kinetic model of intracellular lipid peroxidation, Free Radic. Biol. Med. 8 (1990) 471–485.
[95] L. Iuliano, J.Z. Pedersen, G. Rotilio, D. Ferro, F. Violi, A potent chain-breaking antioxidant activity of the cardiovascular drug dipyridamole, Free Radic. Biol. Med. 18 (1995) 239–247.
[96] E. Niki, T. Saito, A. Kawakami, Y. Kamiya, Inhibition of oxidation of methyl linoleate in solution by vitamin E and vitamin C, J. Biol. Chem. 259 (1984) 4177–4182.
[97] R. Radi, A. Denicola, B. Alvarez, G. Ferrer, H. Rubbo, The biological chemistry of peroxynitrite, in: L.J. Ignarro (Ed.), Nitric Oxide Biology and Pathobiology, Academic Press, 2000, pp. 57–82.
[98] E. Mvula, M.N. Schuchmann, C. von Sonntag, Reactions of phenol-OH-adduct radicals. Phenoxyl radical formation by water elimination vs. oxidation by dioxygen, J. Chem. Soc. Perkin Trans. 2 (2001) 264–268.
[99] G. Merenyi, J. Lind, Free radical formation in the peroxynitrous acid (ONOOH)/peroxynitrite (ONOO-) system, Chem. Res. Toxicol. 11 (1998) 243–246.
[100] S. Goldstein, G. Czapski, J. Lind, G. Merenyi, Mechanism of deomposition of peroxynitric ion (O2NOO-): evidence for the formation of O2.- and.NO2 radicals, Inorg. Chem. 1998 (1998) 3943–3947.
[101] M. Sturzbecher, R. Kissner, T. Nauser, W.H. Koppenol, Homolysis of the peroxynitrite anion detected with permanganate, Inorg. Chem. 46 (2007) 10655–10658.
[102] J.W. Coddington, J.K. Hurst, S.V. Lymar, Hydroxyl radical formation during peroxynitrous acid decomposition, J. Am. Chem. Soc. 121 (1999) 2438–2443.
[103] G. Merenyi, J. Lind, S. Goldstein, G. Czapski, Peroxynitrous acid homolyzes into *OH and *NO2 radicals, Chem. Res. Toxicol. 11 (1998) 712–713.
[104] W.G. Mallard, A.B. Ross, W. Helman, NIST Standard References Database 40, Version 3, 1998.
[105] S. Goldstein, G. Czapski, J. Lind, G. Merenyi, Effect of *NO on the decomposition of peroxynitrite: reaction of N2O3 with ONOO, Chem. Res. Toxicol. 12 (1999) 132–136.
[106] J.L. Caulfield, S.P. Singh, J.S. Wishnok, W.M. Deen, S.R. Tannenbaum, Bicarbonate inhibits N-nitrosation in oxygenated nitric oxide solutions, J. Biol. Chem. 271 (1996) 25859–25863.
[107] C. Molina, R. Kissner, W.H. Koppenol, Decomposition kinetics of peroxynitrite: influence of pH and buffer, Dalton Trans. 42 (2013) 9898–9905.
[108] J.P. Eiserich, J. Butler, A. van der Vliet, C.E. Cross, B. Halliwell, Nitric oxide rapidly scavenges tyrosine and tryptophan radicals, Biochem. J. 310 (Pt 3) (1995) 745–749.